NAVAL POSTGRADUATE SCHOOL
Monterey, California

THESIS

DAMPING IN STIFFENER WELDED STRUCTURES

by

Charles W. Ehnes

June 2003

Thesis Advisor:	Young S. Shin
Co-Advisor:	Ilbae Ham

Approved for public release, distribution is unlimited

THIS PAGE INTENTIONALLY LEFT BLANK

REPORT DOCUMENTATION PAGE			Form Approved OMB No. 0704-0188
Public reporting burden for this collection of information is estimated to average 1 hour per response, including the time for reviewing instruction, searching existing data sources, gathering and maintaining the data needed, and completing and reviewing the collection of information. Send comments regarding this burden estimate or any other aspect of this collection of information, including suggestions for reducing this burden, to Washington headquarters Services, Directorate for Information Operations and Reports, 1215 Jefferson Davis Highway, Suite 1204, Arlington, VA 22202-4302, and to the Office of Management and Budget, Paperwork Reduction Project (0704-0188) Washington DC 20503.			
1. AGENCY USE ONLY *(Leave blank)*	**2. REPORT DATE** June 2003	**3. REPORT TYPE AND DATES COVERED** Master's Thesis	
4. TITLE AND SUBTITLE: Damping in Stiffener Welded Structures			**5. FUNDING NUMBERS**
6. AUTHOR(S) Charles W. Ehnes			
7. PERFORMING ORGANIZATION NAME(S) AND ADDRESS(ES) Naval Postgraduate School Monterey, CA 93943-5000			**8. PERFORMING ORGANIZATION REPORT NUMBER**
9. SPONSORING /MONITORING AGENCY NAME(S) AND ADDRESS(ES) N/A			**10. SPONSORING/MONITORING AGENCY REPORT NUMBER**
11. SUPPLEMENTARY NOTES The views expressed in this thesis are those of the author and do not reflect the official policy or position of the Department of Defense or the U.S. Government.			
12a. DISTRIBUTION / AVAILABILITY STATEMENT Approved for public release, distribution is unlimited			**12b. DISTRIBUTION CODE**

13. ABSTRACT ***(maximum 200 words)***

Damping of welded structures is a subject of great interest and application for the navy as relates to ship shock survivability and acoustic transmission of ship noise. The purpose of this research is to study the effects of welding on damping. A generic model of a warship's hull structure was used to study damping effects. The model's natural frequencies and mode shapes were calculated using a finite element model prior to model testing. The frequency response and natural frequencies of the model were determined experimentally by exciting the model and measuring the response throughout the structure using Frequency Response Functions (FRF's). The results were compared with the finite element modeling. The damping ratio of the model in relation to position from excitation was calculated using the half-power point method and then a more detailed analysis of frequency dependent damping versus position was made using modal parameter extraction using the Complex Exponential Method.

14. SUBJECT TERMS Vibration, Damping, Welding			**15. NUMBER OF PAGES** 67
			16. PRICE CODE
17. SECURITY CLASSIFICATION OF REPORT Unclassified	**18. SECURITY CLASSIFICATION OF THIS PAGE** Unclassified	**19. SECURITY CLASSIFICATION OF ABSTRACT** Unclassified	**20. LIMITATION OF ABSTRACT** UL

NSN 7540-01-280-5500 Standard Form 298 (Rev. 2-89)
Prescribed by ANSI Std. 239-18

THIS PAGE INTENTIONALLY LEFT BLANK

Approved for public release, distribution is unlimited

DAMPING IN STIFFENER WELDED STRUCTURES

Charles W. Ehnes
Lieutenant, United States Navy
B.S.O.E., United States Naval Academy, 1996

Submitted in partial fulfillment of the
requirements for the degree of

MASTER OF SCIENCE IN MECHANICAL ENGINEERING

from the

NAVAL POSTGRADUATE SCHOOL
June 2003

Author: Charles W. Ehnes

Approved by: Young S. Shin
Thesis Advisor

Ilbae Ham
Co-Advisor

Young W. Kwon
Chairman, Department of Mechanical Engineering

THIS PAGE INTENTIONALLY LEFT BLANK

ABSTRACT

Damping of welded structures is a subject of great interest and application for the navy as relates to ship shock survivability and acoustic transmission of ship noise. The purpose of this research is to study the effects of welding on damping. A generic model of a warship's hull structure was used to study damping effects. The model's natural frequencies and mode shapes were calculated using a finite element model prior to model testing. The frequency response and natural frequencies of the model were determined experimentally by exciting the model and measuring the response throughout the structure using Frequency Response Functions (FRF's). The results were compared with the finite element modeling. The damping ratio of the model in relation to position from excitation was calculated using the half-power point method and then a more detailed analysis of frequency dependent damping versus position was made using modal parameter extraction using the Complex Exponential Method.

THIS PAGE INTENTIONALLY LEFT BLANK

TABLE OF CONTENTS

THIS PAGE INTENTIONALLY LEFT BLANK

LIST OF FIGURES

THIS PAGE INTENTIONALLY LEFT BLANK

LIST OF TABLES

THIS PAGE INTENTIONALLY LEFT BLANK

ACKNOWLEDGMENTS

I would like to thank Professor Young Shin and Dr. Ilbae Ham for their guidance and insight into the world of vibration and damping. Their support and guidance was invaluable in the successful completion of my thesis.

To Tom Christensen and Sheila Deiotte, without your technical support helping with instrumentation this project would have been impossible.

To my wife Karou, your love and unwavering support have given me strength and buoyed my spirits throughout the countless hours in pursuit of my Masters Degree. Thank you for everything.

To ENS Jon Erskine, my office-mate and fellow vibration/damping student, working with you has helped me learn more than I could have had I been working alone. Good luck once you hit the Fleet and keep your powder dry!

THIS PAGE INTENTIONALLY LEFT BLANK

I. INTRODUCTION

A. BACKGROUND

Damping of ship structures is a subject of great interest and application for the navy as it relates to ship shock survivability and acoustic transmission of ship noise. The concept of damping can be thought of as the culmination of various energy dissipation mechanisms that remove mechanical energy from a vibrating system. The energy dissipation mechanisms can be broadly categorized into two categories, hydrodynamic effects and structural damping of the ship hull. While some study has gone into the hydrodynamic effected hull damping, little study has gone into structural damping in the ship hull. The ship system has many proposed energy dissipation sources such as welded joints and stiffeners, long cable trays, hangers, snubbers, etc. This thesis focuses on the effect of welds in the ship's structure to the total damping of the ship structure system.

Betts and his colleagues conducted a survey of internal hull damping, and they concluded that welding effects together with stress concentrations were among the most important sources of hull damping in deformation modes [Ref 1]. Figure 1 shows a typical plot for the damping properties of mild steel in terms of the specific damping strain energy, for a wide range of stress amplitudes.

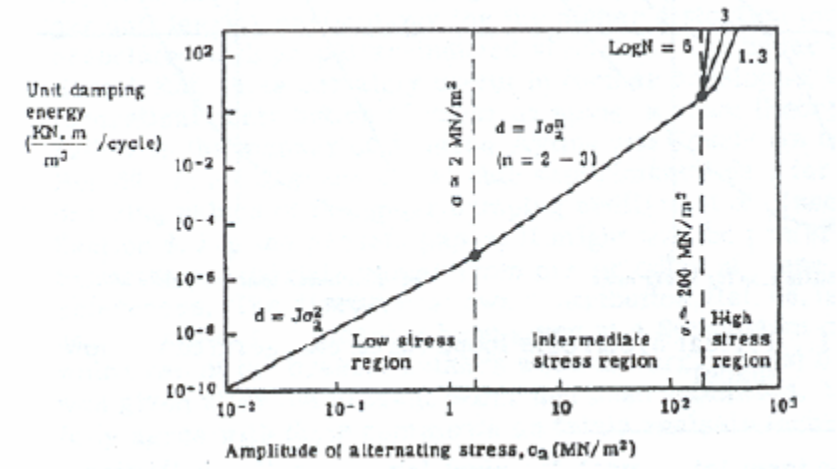

Figure 1. Unit Damping Energy vs. Stress Amplitude (from Ref 7)

Damping curves for other metallic materials generally have similar forms to those of mild steel. As shown in Figure 1, as stress amplitude increases, damping energy

increases. The primary effect of welding is from contraction of the weld upon cooling. This contraction causes tensile yield stresses in the material parallel and adjacent to the weld. The area of residual tensile yield stress at fillet welds usually extends for approximately 3 to 4 ½ thicknesses on either side of the weld, leaving some 10-15% of the plate material at tensile yield stress [Ref. 1]. Betts suggests that the residual stresses will frequently be in the plastic region and that vibratory motion of the weld will cause plastic strain, considerably increasing the damping of the structure. Imperfect welds where there are gaps between the materials was also believed to give rise to dry friction between the materials creating another source of damping.

In thesis work done by Carey [Ref. 2] research was conducted of the welding effects on damping in several beam-stiffened plates. At frequencies below 500 Hz, the trend found was that welding caused an increase in damping in the plates. The results of these tests however were not consistent and not precise enough to quantify the damping attributed to weld effects. In a continuation of work done by Carey, this thesis continues examination of weld effects on damping in a more complicated structure that contains larger amounts of welded surface, better representing a ship's hull.

B. OBJECTIVES

The objective of this research was to investigate the damping effects of welds in a beam-stiffened plate gaining insight on damping effects of welds in a ship's hull structure. A more complete understanding of structural damping in ship structures may improve computer simulations of ship vibration in ship-shock trials and produce opportunities to reduce acoustic transmission of ship noise.

II. THEORY

A. DAMPING MODEL ASSUMPTIONS

As previously suggested in the background section, the origins of ship structural damping are believed to lie in material hysteresis and dry friction at joints. Hysteretic damping comes from imperfections in real materials that cause energy to be absorbed during cycling, while Coulomb damping comes from the dry friction at joints. Recognizing the damping mechanisms of the system come from a combination of Hysteretic and Coulomb as well as Viscous damping, a fairly accurate mathematical representation can be made by assuming only viscous damping. This assumption makes calculation of damping properties of the model less burdensome while still maintaining a good approximation to the true total damping of the model [Ref. 3].

Another assumption made to make damping calculations less burdensome was to assume the system experiences linear proportional damping, the damping of the system being linearly proportional to the mass and the stiffness of the system. For a multi-degree-of-freedom system such as a ship hull, these assumptions lead to the following damping equation;

$$[C] = \alpha[M] + \beta[K] \tag{1}$$

These assumptions form the basis for the model by which the damping values for the ship hull model were calculated.

B. VISCOUS DAMPING

Viscous damping can be expressed by the following equation

$$F_d = c\dot{x} \tag{2}$$

where c is a constant of proportionality

The equation of motion for a damped single degree of freedom (SDOF) system experiencing free vibration is:

$$m\ddot{x} + c\dot{x} + kx = F(t) \tag{3}$$

Where m = Mass constant
c = Damping constant
k = Stiffness constant

x = Displacement of the system
$\dot{x}$ = Velocity of the system
$\ddot{x}$ = Acceleration of the system
$F(t)$ = Force applied to the system

The homogenous solution ($F(t)=0$) of the differential equation of motion, (equation (3)) is found by assuming $x=e^{st}$. Substituting into the differential equation yields:

$$(ms^2+cs+k)e^{st}=0 \tag{4}$$

which is satisfied for all values of t when

$$s^2+\frac{c}{m}s+\frac{k}{m}=0 \tag{5}$$

the two roots of this characteristic equation are:

$$s_{1,2}=-\frac{c}{2m}\pm\sqrt{\left(\frac{c}{2m}\right)^2-\frac{k}{m}} \tag{6}$$

Thus the general solution of the differential equation is:

$$x=Ae^{s_1t}+Be^{s_2t} \tag{7}$$

where A and B are constants evaluated from the initial conditions of displacement and velocity at time zero ($x(0)$ and $\dot{x}(0)$). Substituting equation (6) into equation (7) produces:

$$x=e^{-(c/2m)t}\left(Ae^{\left(\sqrt{(c/2m)^2-k/m}\right)t}+Be^{\left(\sqrt{(c/2m)^2-k/m}\right)t}\right) \tag{8}$$

When the damping term $(c/2m)^2$ is more than (k/m), the over damped case will occur, the exponents in (8) being real numbers and thus leading to no oscillations. If the damping term is less than (k/m), the exponents will become imaginary numbers leading to the under damped case and oscillatory motion. When $(c/2m)^2=k/m$ and the radical is equal to zero the case is known as critical damping, c_c and leads to one oscillation cycle

$$c_c=2m\sqrt{\frac{k}{m}}=2m\omega_n=2\sqrt{km} \tag{9}$$

Any damping can be expressed in terms of the critical damping by a non-dimensional number ζ, the damping ratio, where $\zeta = \frac{c}{c_c}$. Hence equation (6) becomes

$$s_{1,2} = \left(-\zeta \pm \sqrt{\zeta^2 - 1}\right)\omega_n \tag{10}$$

and the differential equation of motion (equation (3)) can now be expressed

$$\ddot{x} + 2\zeta\omega_n\dot{x} + \omega_n = \frac{1}{m}F(t) \tag{11}$$

[Ref. 3]

C. FORCED VIBRATION

To accurately calculate the damping in a structure, its frequency response must be determined in order to obtain the natural frequencies of the structure. In any liner system, there is a direct liner relationship between the input signal and the output signal; the ratio of this relationship is termed the Frequency Response Function, H(ω).

As previously stated, the equation of motion for a single degree-of-freedom system (1-DOF), is:

$$m\ddot{x} + c\dot{x} + kx = F(t) \tag{3}$$

To solve the differential equation, we let the input $F(t) = e^{i\omega t}$. The steady-state output will be $x = H(\omega)e^{i\omega t}$, where ω is the frequency of the applied force and t is time and $H(\omega)$ is a complex function. The steady-state output equation is differentiated, to get expressions for the velocity and acceleration. These expressions for displacement, velocity and acceleration are substituted into equation (3) and canceling like terms the following is obtained:

$$(-m\omega^2 + ic\omega + k)H(\omega) = 1 \tag{12}$$

Then the frequency response equation becomes:

$$H(\omega) = \frac{1}{k - m\omega^2 + ic\omega} \tag{13}$$

By factoring the stiffness from the denominator and substituting the following equations into equation (3),

$$\omega_n^2 = \frac{k}{m} \qquad \zeta = \frac{c}{c_c} = \frac{c}{2\sqrt{km}} \tag{14}$$

ω_n = Natural frequency
ζ = Damping ratio
c_c = Critical damping coefficient

the frequency response can then be written in its classical form:

$$H(\omega) = \frac{1}{1 - \left(\omega/\omega_n\right)^2 + i2\zeta\left(\omega/\omega_n\right)} \tag{15}$$

For a 1-DOF system, there is one natural frequency and one damping ratio associated with it. For multiple degrees-of-freedom (N-DOF), there are as many natural frequencies and damping ratios as there are DOF. Modal analysis can be used to analyze a N-DOF system. The equations of motion for a N-DOF system in matrix form is:

$$[M]\{\ddot{x}\} + [C]\{\dot{x}\} + [K]\{x\} = \{F\} \tag{16}$$

The mass, damping, and stiffness matrices are *n* x *n* matrices, where *n* is the number of DOF in the system. The force, displacement, velocity and acceleration vectors are *n* by 1 in size. Each element in the vectors corresponds to a DOF of the system. The mass and stiffness matrixes are symmetric and may have some form of coupling. The first step to analyze the multi-DOF system is to determine the natural frequencies and mode shapes by analyzing the free response of the system. The general form of the free response of motion for a N-DOF system is as follows:

$$[M]\{\ddot{x}\} + [K]\{x\} = \{0\} \tag{17}$$

For each of the DOF we use $x = Xe^{i\omega t}$ and equation (17) reduces to:

$$\left[K_{ij} - M_{ij}\omega^2\right]\{X\} = 0 \qquad \text{where } i = 1 \ldots n \text{ and } j = 1 \ldots n \tag{18}$$

The indices *i* and *j* correspond to the element locations in the mass and stiffness matrices. From equation (18), a solution of the displacements is $\{X\} = 0$ if the matrix $\left[K_{ij} - M_{ij}\omega^2\right]$ is invertible. This solution, however, is the trivial solution. To ensure that the matrix is not invertible, the determinant of the matrix is forced to equal zero. By forcing the matrix determinant to equal zero, the matrix will be singular and an inverse matrix does not exist, thus a non-trivial solution can be found. The eigenvalues found for

the matrix are the system's natural frequencies and the eigenvectors found are the system's mode shapes. The mode shapes of the system illustrate how the system responds to an excitation at the corresponding natural frequency. The system's modal matrix is formed by placing the mode shape vectors as the columns of the matrix.

$$[\Phi] = \left[\{\phi\}^1 \{\phi\}^2 .... \{\phi\}^n \right] \tag{19}$$

Φ is the modal matrix and ϕ are the mode shape vectors. The modal matrix will have the same number of the rows as there are DOF's. To decouple equation (16), we assume a set of modal coordinates:

$$\{x\} = [\Phi]\{q\}, \ \{\dot{x}\} = [\Phi]\{\dot{q}\}, \ \{\ddot{x}\} = [\Phi]\{\ddot{q}\} \tag{20}$$

next substitute equation (20) into equation (16) and multiply both sides by the transpose of the modal matrix.

$$[\Phi]^T [M][\Phi]\{\ddot{q}\} + [\Phi]^T [C][\Phi]\{\dot{q}\} + [\Phi]^T [K][\Phi]\{q\} = [\Phi]^T \{F\} \tag{21}$$

Using the orthogonal properties of the modal matrix and the symmetric properties of the mass, damping and stiffness matrix results in the following equation:

$$[\tilde{m}_{ii}]\{\ddot{q}\} + [\tilde{c}_{ii}]\{\dot{q}\} + \left[\tilde{k}_{ii}\right]\{q\} = [\Phi]^T \{F\} \tag{22}$$

The new modal mass, damping, and stiffness matrixes are diagonal. As a result, the modal coordinates are decoupled and can be solved for each Degree of Freedom in the same manner as a 1-DOF system. Equation (22) can be further simplified by multiplying both sides by the inverse of the modal mass matrix to get:

$$\{\ddot{q}\} + [2\zeta_{ii}\omega_{ii}]\{\dot{q}\} + \left[\omega_{ii}^2\right]\{q\} = \left\{\tilde{F}\right\} \tag{23}$$

where $\left\{\tilde{F}\right\} = [\tilde{m}]^{-1} [\Phi]^T \{F\}$.

[Ref. 3 and 4]

D. DAMPING CALCULATION: HALF-POWER POINT METHOD

The damping ratio can be calculated experimentally by using the half-power point method. The half-power point method determines the damping ratio by examining the sharpness of the resonance peak. The following equation is the magnitude of the frequency response:

$$H = \frac{1}{\sqrt{\left[1-\left(\omega/\omega_n\right)^2\right]^2 + \left[2\zeta\left(\omega/\omega_n\right)\right]^2}} \tag{24}$$

At resonance, $\left(\omega/\omega_n = 1\right)$ the magnitude of the frequency response is $H_{res} = \frac{1}{2\zeta}$. Taking the square of both sides of equation (24):

$$\left(\frac{1}{2\zeta}\right)^2 = \frac{1}{\left[1-\left(\frac{\omega}{\omega_n}\right)^2\right]^2 + \left[2\zeta\left(\frac{\omega}{\omega_n}\right)\right]^2} \tag{25}$$

or

$$\left(\frac{\omega}{\omega_n}\right)^4 - 2\left(1-2\zeta^2\right)\left(\frac{\omega}{\omega_n}\right)^2 + \left(1-8\zeta^2\right) = 0$$

Solving for $\left(\omega/\omega_n\right)^2$ results in the following equation:

$$\left(\frac{\omega}{\omega_n}\right)^2 = \left(1-2\zeta^2\right) \pm 2\zeta\sqrt{1-\zeta^2} \tag{26}$$

Assuming that $\zeta \ll 1$, the higher order terms can be neglected, resulting in the following equation:

$$\left(\frac{\omega}{\omega_n}\right)^2 = 1 \pm 2\zeta \tag{27}$$

Letting ω_1 and ω_2 correspond to the roots of equation (27) and $\omega_2 > \omega_1$, equation (27) becomes:

$$4\zeta = \frac{\omega_2^2 - \omega_1^2}{\omega_n^2} \cong 2\left(\frac{\omega_2 - \omega_1}{\omega_n}\right) \tag{28}$$

The damping ratio can now be determined by rearranging equation (28):

$$\zeta = \frac{\omega_2 - \omega_1}{2\omega_n} = \frac{f_2 - f_1}{2f_n} \tag{29}$$

Figure 2 illustrates how the half-power point method is utilized. [Ref. 1]

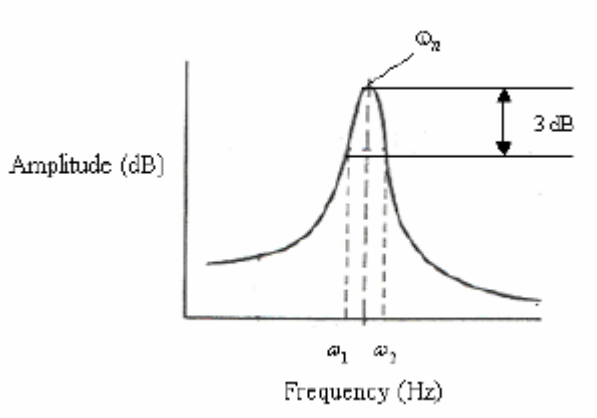

Figure 2. Half-power point method [Ref. 1]

E. DAMPING CALCULATION: COMPLEX EXPONETIAL METHOD

The Complex Exponential Method (CEM) is used to extract modal parameters of a system directly from the system response data. The Receptance FRF (displacement/force) $\alpha(\omega)$, of a viscously damped general MDOF system can be represented as:

$$\alpha(\omega) = \sum_{r=1}^{N}\left(\frac{A_r}{j\omega - s_r} + \frac{A_r^*}{j\omega - s_r^*}\right); \text{ where } s_r = -\omega_r\zeta_r + j\omega_r\sqrt{1-\zeta_r^2} \tag{30}$$

or

$$\alpha(\omega) = \sum_{r=1}^{2N}\frac{A_r}{j\omega - s_r} \;;\; s_r \to s_r^*,\; A_r \to A_r^*, \text{ for } r > N$$

and Mobility (velocity/force) $Y(\omega)$ can be related to $\alpha(\omega)$,

$$Y(\omega) = j\omega\alpha(\omega) \tag{31}$$

From classical theory, the corresponding Impulse Response Function (IRF), $h(t)$ can be obtained by taking the Inverse Fourier Transform (IFT) of the Receptance $\alpha(\omega)$:

$$h(t) = \sum_{r=1}^{2N} A_r e^{s_r t} \tag{32}$$

The velocity form of IRF can be expressed as:

$$\dot{h}(t) = \sum_{r=1}^{2N} A_r s_r e^{s_r t} \tag{33}$$

Then the sampled velocity data set can be expressed as follows:

$$\dot{h}_0, \dot{h}_1, \dot{h}_2, ..., \dot{h}_q = \dot{h}(0), \dot{h}(\Delta t), \dot{h}(2\Delta t), ..., \dot{h}(q\Delta t) \tag{34}$$

Using the following simplified notation,

$$e^{s_r \Delta t} \to V_r \tag{35}$$

Thus for the j[th] sample data of equation (33) is expressed as:

$$\dot{h}_j = \dot{h}(\cancel{j\Delta t}) = \sum_{r=1}^{2N} A_r s_r V_r (\cancel{j\Delta t}) = \sum_{r=1}^{2N} A_r s_r V_r \tag{36}$$

When extended to the full data set of q samples, equation (36) gives:

$$\begin{aligned}
\dot{h}_0 &= s_1 A_1 + s_2 A_2 + \cdots + s_{2N} A_{2N} \\
\dot{h}_1 &= V_1 s_1 A_1 + V_2 s_2 A_2 + \cdots + V_{2N} s_{2N} A_{2N} \\
\dot{h}_2 &= V_1^2 s_1 A_1 + V_2^2 s_2 A_2 + \cdots + V_{2N}^2 s_{2N} A_{2N} \\
&\vdots \qquad \vdots \qquad \vdots \qquad \vdots \\
\dot{h}_q &= V_1^q s_1 A_1 + V_2^q s_2 A_2 + \cdots + V_{2N}^q s_{2N} A_{2N}
\end{aligned} \tag{37}$$

Given that the number of sample points q exceeds 4N, this equation can be used to set up an eigenvalue problem and the solution yields the complex natural frequencies contained in the parameters V_1, V_2, etc….

Multiplying each equation in (37) by a coefficient, β_j forms the following set of equations:

$$\begin{aligned}
\beta_0 h_0 &= \beta_0 A_1 + \beta_0 A_2 + \cdots + \beta_0 A_{2N} \\
\beta_1 h_1 &= \beta_1 V_1 A_1 + \beta_1 V_2 A_2 + \cdots + \beta_1 V_{2N} A_{2N} \\
\beta_2 h_2 &= \beta_2 V_1^2 A_1 + \beta_2 V_2^2 A_2 + \cdots + \beta_2 V_{2N}^2 A_{2N} \\
&\vdots \qquad \vdots \qquad \vdots \qquad \vdots \\
\beta_q h_q &= \beta_q V_1^q A_1 + \beta_q V_2^q A_2 + \cdots + \beta_q V_{2N}^q A_{2N}
\end{aligned} \tag{38}$$

Adding all equation in (38) results in:

$$\sum_{i=0}^{q} \beta_i \dot{h}_i = \sum_{j=1}^{2N} (A_j \sum_{i=0}^{q} \beta_i V_j^i) \tag{39}$$

The coefficients β_j are taken to be the coefficients in the equation,

$$\beta_0 + \beta_1 V + \beta_2 V^2 + \beta_3 V^3 + \cdots + \beta_q V^q = 0 \tag{40}$$

for which the roots are $V_1, V_2, \ldots, V_q$.

The values of the β coefficients are sought to determine the roots of (40), the values of V_r and thus the system natural frequencies. With q being the number of degrees of freedom of the system model, we can set these two parameters to the same value, i.e. let q=2N.

The equation (40) can now be expressed as:

$$\sum_{j=0}^{2N} \beta_j V_r^j = 0 \text{ ; for r=1, 2N} \tag{41}$$

and thus every term on the right-hand side of equation (39) is zero.

$$\sum_{i=0}^{2N} \beta_i \dot{h}_i = 0 \tag{42}$$

rearranging equation (42), by setting $\beta_{2N} = 1$

$$\sum_{i=0}^{2N-1} \beta_i \dot{h}_i = -\dot{h}_{2N} \tag{43}$$

Repeating the process from (34) to (43) using different sets of IRF data points and further choosing new data sets that overlaps, successive applications of this procedure lead to a full set of 2N equations:

$$\begin{bmatrix} \dot{h}_0 & \dot{h}_1 & \dot{h}_2 & \cdots & \dot{h}_{2N-1} \\ \dot{h}_1 & \dot{h}_2 & \dot{h}_3 & \cdots & \dot{h}_{2N} \\ \vdots & \vdots & \vdots & \ddots & \vdots \\ \dot{h}_{2N-1} & \dot{h}_{2N} & \dot{h}_{2N+1} & \cdots & \dot{h}_{4N-2} \end{bmatrix} \begin{Bmatrix} \beta_0 \\ \beta_1 \\ \vdots \\ \beta_{2N-1} \end{Bmatrix} = - \begin{Bmatrix} \dot{h}_{2N} \\ \dot{h}_{2N+1} \\ \vdots \\ \dot{h}_{4N-1} \end{Bmatrix} \tag{44}$$

or

$$\left[\dot{h}\right]_{2N\times 2N} \{\beta\}_{2N\times 1} = -\left\{\tilde{h}\right\}_{2N\times 1} \tag{45}$$

The unknown coefficients $\{\beta\}$ can be found from equation (45). The values of $V_1, V_2, \ldots, V_{2N}$ can now be determined using equation (40) and subsequently the system natural frequencies can be found using the relationship.

$$V_r = e^{s_r \Delta t} \tag{35}$$

Using equation (37), corresponding modal constants, $A_1, A_2, \ldots, A_{2N}$ can be calculated. This may be written as:

$$\begin{bmatrix} 1 & 1 & 1 & \cdots & 1 \\ V_1 & V_2 & V_3 & \cdots & V_{2N} \\ V_1^2 & V_1^2 & V_1^2 & \cdots & V_{2N}^2 \\ \vdots & \vdots & \vdots & \ddots & \vdots \\ V_1^{2N-1} & V_2^{2N-1} & V_3^{2N-1} & \cdots & V_{2N}^{2N-1} \end{bmatrix} \begin{Bmatrix} A_1 s_1 \\ A_2 s_2 \\ A_3 s_3 \\ \vdots \\ A_{2N} s_{2N} \end{Bmatrix} = \begin{Bmatrix} \dot{h}_0 \\ \dot{h}_1 \\ \dot{h}_2 \\ \vdots \\ \dot{h}_{2N-1} \end{Bmatrix} \tag{46}$$

or

$$[V]\{A\} = \{h\} \tag{47}$$

[Ref. 5]

F. VERIFICATION OF EXTRACTED MODAL PARAMETERS

The modal parameters calculated from the above procedure can be verified by comparing synthesized time histories to the originally measured time histories. From equations (30) and (31),

$$\hat{Y}(\omega) = \sum_{r=1}^{N} \left(\frac{j\omega A_r}{j\omega - s_r} + \frac{j\omega A_r^*}{j\omega - s_r^*} \right); \qquad s_r = -\omega_r \zeta_r + j\omega_r \sqrt{1-\zeta_r^2} \tag{48}$$

or

$$\hat{Y}(\omega) = \sum_{r=1}^{2N} \frac{j\omega A_r}{j\omega - s_r}; \;\; s_r \to s_r^*, \; A_r \to A_r^*, \text{ for } r > N \tag{49}$$

Mobility can be calculated and by inverse FFT, taking the real part of the results, synthesized IRF can be calculated and compared to original time histories. [Ref. 5]

$$\left\{ \hat{\dot{h}} \right\} = \text{Real of IFFT } (\Delta f \;\; \hat{Y}) \tag{50}$$

G. CALCULATION OF RAYLEIGH DAMPING

Using Rayleigh damping representation, the damping matrix can be represented as:

$$[C] = \alpha [M] + \beta [K] \tag{1}$$

by using the mass normalized modal matrix $[\phi]$, the damping matrix may we rewritten:

$$[\phi]^T [C][\phi] = [2\omega_r \zeta_r]_{diag} = \alpha [I] + \beta \left[\omega_r^2 \right]_{diag} \tag{51}$$

By using equation (51) for all 2N modes, following 2N equations can be set.

$$\begin{aligned} \alpha + \beta\omega_1^2 &= 2\omega_1\zeta_1 \\ \alpha + \beta\omega_2^2 &= 2\omega_2\zeta_2 \\ &\vdots \\ \alpha + \beta\omega_{2N}^2 &= 2\omega_{2N}\zeta_{2N} \end{aligned} \tag{52}$$

or

$$[W]_{2N\times 2}\begin{Bmatrix}\alpha\\ \beta\end{Bmatrix} = \{Z\}_{2N\times 1} \tag{53}$$

From equation (53), the two parameters α and β are calculated in a least squares solution by matrix pseudo-inversion. [Ref. 5]

$$\begin{Bmatrix}\alpha\\ \beta\end{Bmatrix} = \left([W]_{2\times 2N}^T [W]_{2N\times 2}\right)^{-1} [W]_{2\times 2N}^T \{Z\}_{2N\times 1} \tag{54}$$

THIS PAGE INTENTIONALLY LEFT BLANK

III. EXPERIMENTAL SETUP

A. EQUIPMENT DESCRIPTION

The equipment used during testing was as follows:

- 8.5 ft x 4 ft "Hull model" panel
- 8.5 ft x 1.5 ft flat panel
- Hewlett Packard 3562A Dynamic Signal Analyzer
- PCB Piezotronics Modally Tuned Impact Hammer
- PCB Piezotronics model 336C04 Accelerometers
- PCB Piezotronics model 208C01 Force Sensor
- PCB Piezotronics model 483B07 Power Unit Amplifier
- MB Dynamics model A SS250VCF Amplifier
- MB Dynamics Modal 50 Exciter
- Modified PC computer with National Instruments "LabVIEW" software

Experimental testing was conducted on a stiffened metal panel matching a ¼ scale section of generic warship hull structure. The model plate was 4 ft by 8.5 ft, 11 gauge A-36 steel and was stiffened length-wise and around the plate edges by 1 inch high 17 gauge A-36 steel strips with 3 inch spacing from the edge of the plate and 6 inch periodic spacing between stiffeners. Transverse stiffeners were 1.75 inch high 14 gauge A-36 steel strips with 3 inch spacing from the edge and 24 inch periodic spacing. Stiffeners were double filet welded to the plate. The hull model was freely suspended from an H-frame by a series of nylon straps hooked to steel rings welded to the structure.

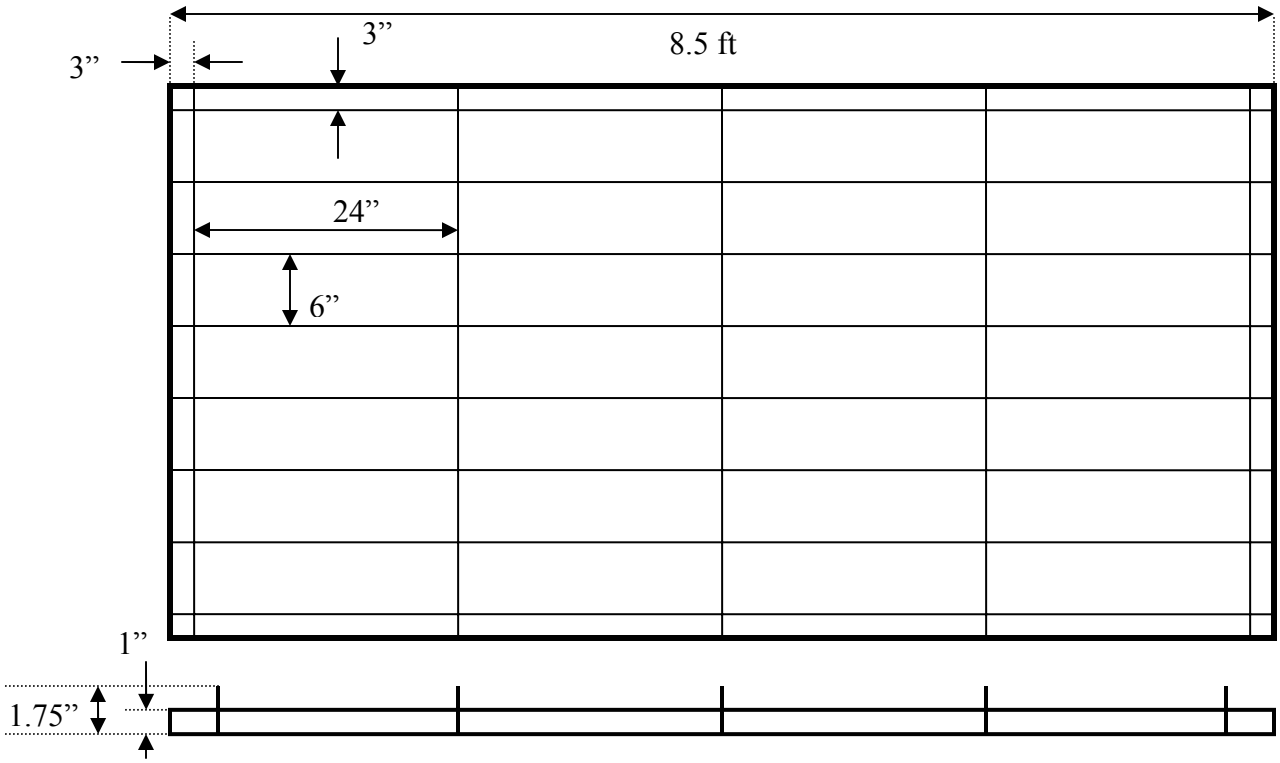

Figure 3. Schematic of hull model

Figure 4. Photo of panel

A section of flat panel 1.5 ft by 8.5 ft, of 4 gauge A-36 steel was tested to be used as a reference to compare with the behavior of the multi-weld “hull panel”. The flat plate was similarly suspended by a series of bungee cords to simulate a free system

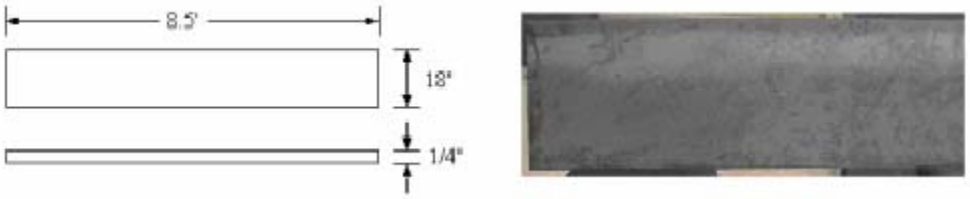

Figure 5. Schematic of Flat Panel model and photo of panel

The Hewlett Packard 3562A Dynamic Signal Analyzer (DSA) was used to compute the frequency response of the panels and as a signal generator. The DSA is a dual-channel, fast Fourier transform-based network, spectrum and waveform analyzer that provides analysis capabilities in both the time and frequency domains. Two input channel and a built –in signal source (noise and sine signals) can be used to perform spectrum analysis. The DSA has a frequency resolution of 25.6 μHz allowing the user to obtain highly accurate, high-resolution plots of the frequency responses of the mechanical system. Single channel accuracy is ±0.15 dB with 80 dB of dynamic range [Ref. 6].

The Piezotronics Modally Tuned Impact Hammer was the series 086B03 model. The modally tuned hammer is capable of exciting structural resonances up to 10 KHz and has a sensitivity of 10 mV/lbf. The hammer converts a transfer force into an electrical signal which was then used by the DSA as the input response. The input signal was obtained from a force transducer on the head of the impact hammer.

The Piezotronics model 336C04 Accelerometers are hermetically sealed, shear structured ICP accelerometers. The accelerometers provide a 10 mV/g output over a frequency range from 1 to20,000 Hz (±10%).

PCB Piezotronics model 208C01 Force Sensor was used to measure exciter force input into the test panel. The force sensor is an ICP Quartz Force Sensor and measures in a range from 10 lbf tension to 10 lbf compression with a sensitivity of 502.5 mV/lbf [Ref. 7 and Ref 8].

The PCB Piezotronics model 483B07 Power Unit Amplifier is a 12 channel amplifier that used to amplify the signals from the force sensor and Accelerometers.

The MB Dynamics model A SS250VCF Amplifier was the used to power the Modal 50 Exciter and amplify the input signal into the Exciter.

The MB Dynamics Modal 50 Exciter is a lightweight permanent magnet shaker that provides 50 pounds dynamic force output. The force output from the Exciter was transmitted to the panel through a steel rod threaded into the PCB Piezotronics force sensor that was bolted to the panel.

A Personal Computer with a multi-channel input signal circuit board was used to take the signals from the force sensor and accelerometers via the PCB Piezotronics Power Unit Amplifier. National Instruments "LabVIEW" software was used to pair the force sensor with each of the accelerometers and making fast Fourier transforms on the pairs to measure the magnitude/phase and real/imaginary frequency response and coherence of the single input multi-output system.

B. EQUIPMENT SETUP

1. Impact Testing

For impact testing, the PCB modally tuned impact hammer was used to excite the model while accelerometers (PCB Piezotronics model 336C04) measured the structure's response. The impact hammer test was used to determine the frequency response of the model. The model was impacted at the excitation point and accelerometer readings were taken at a variety of positions on the model. The input and output signals were amplified by the PCB Power unit with input gain set at 1 and output gain set at 10. The input and output signals were analyzed using the Dynamic Signal Analyzer (DSA), where the frequency response and coherency were measured. The force-exponential window was used during the impact hammer test and 10 stable mean averages were used to obtain the frequency response. The time record was set to trigger when the input signal from the hammer reached 0.5 volts. Figure 6 shows the equipment setup for impact hammer testing.

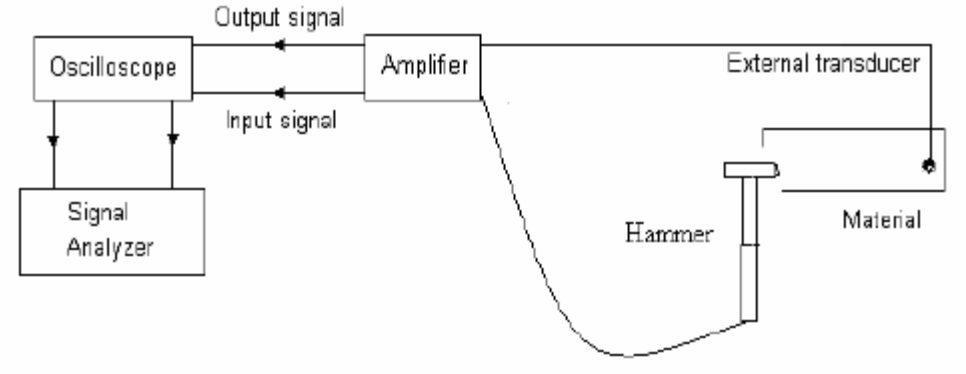

Figure 6. Equipment setup for Impact Hammer Testing

2. Exciter Testing

The Dynamic Signal Analyzer provided a 1 Volt random noise input signal throughout the range of 0-250 Hz via the MB Dynamics amplifier to the MB Dynamics Modal 50 Exciter to excite the panel. The input and output signals were amplified by the PCB Piezotronics Power Unit Amplifier with gain set to 1 for all channels. The input signal was measured by the PCB Piezotronics force sensor bolted to the panel to which the exciter's steel rod was threaded into. PCB Piezotronics accelerometers were used to measure the model response throughout the structure. The signals of the input force sensor and the one output accelerometer were fed to the Digital Signal Analyzer for frequency response, and coherency measurement and the input signal and all 5 output signals were fed to the PC where the National Instruments "LabView" software to measure the magnitude/phase and real/imaginary frequency response and coherence. 10 stable mean averages were used to obtain the model's frequency response and frequency resolution was set to 0.05 Hz. Results were saved as text files for further post-processing. Figure 7 shows a schematic of the experimental setup.

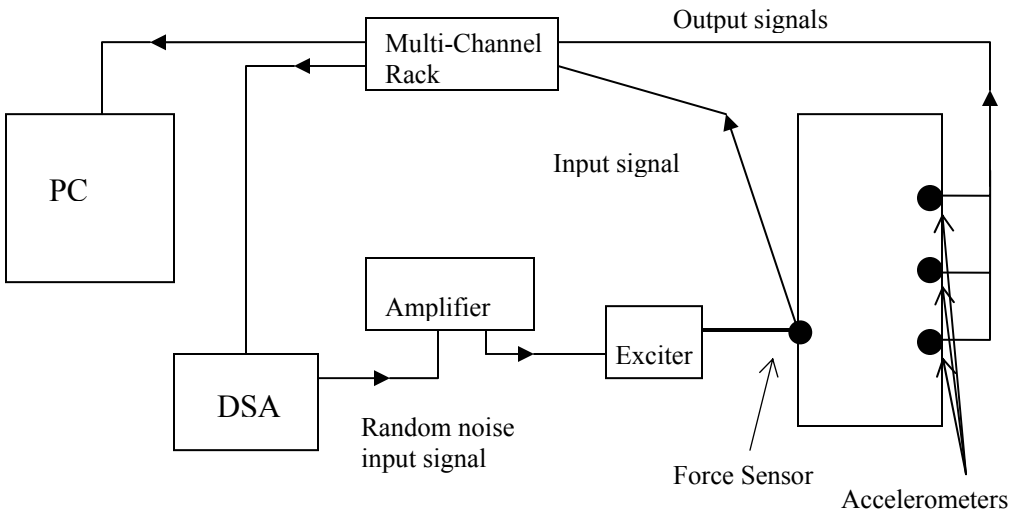

Figure 7. Equipment setup for Exciter Testing

C. FINITE ELEMENT MODEL SIMULATION

In an attempt to relate damping with the mode shape and natural frequency a finite element model was created for hull panel and flat plate. The panel was modeled using 22092 quad 4 shell elements utilizing the MSC Patran/Nastran computer modeling system. No attempt was made to simulate the actual weld of the structure, stiffener and panel surfaces were simply merged together using the equivalence command in Patran. Similarly, the flat plate was modeled using 29376 quad 4 shell elements.

IV. EXPERIMENTAL SETUP AND RESULTS

A. IMPACT HAMMER TESTING

A variety of tips of varying hardness were used with the impact hammer to find which tip produced the best coherence. During testing, an acceptable level of coherency was not able to be achieved using any of the various tips for the impact hammer and impact hammer testing was abandoned in favor of shaker testing which produced much better levels of coherence.

B. EXCITER TESTING

1. Half-Power Point Method

The Half-Power point method was used to make preliminary tests to find the effect damping across the welded panel. For this initial testing the force gage and a single accelerometer were used as the input and output respectively. Figure 7 displays the placement of the force gage and the various placements of the accelerometer across the panel for this preliminary testing.

	A	H	O	V
	B	I	P	W
	C	J	Q	* X
	D	K	R	Y
	E	L	S	Z
	F	M	T	AA
	G	N	U	BB

Figure 8. Exciter (*) and Accelerometer (letters) Placement for Half-Power Point Testing

A 1 Volt random noise signal from the DSA was used as the input signal. The testing frequency range was from 0 to 250 Hz and was averaged 15 times. Figure 8 is a sample frequency plot of the hull panel response.

Through testing a resonant peak was found as approximately 113 Hz throughout the panel. Using a zoom measurement of the 113 Hz frequency range, a more precise measurement of the resonance frequency f_n, and the frequencies f_1 and f_2, 3 decibels below resonance before and after resonance respectively were found. As discussed in the theory section previously, the damping ratio can now be calculated using equation (29)

$$\zeta = \frac{\omega_2 - \omega_1}{2\omega_n} = \frac{f_2 - f_1}{2f_n} \tag{29}$$

Table 1. Half-Power Point Testing Results

$f_2 = 113.137$ A $f_1 = 112.97$ $\zeta = 0.00146$ $f_n = 113.3$	$f_2 = 113.05$ H $f_1 = 112.9$ $\zeta = 0.00133$ $f_n = 113.2$	$f_2 = 112.962$ O $f_1 = 112.817$ $\zeta = 0.00130$ $f_n = 113.11$	$f_2 = 113.1$ V $f_1 = 112.93$ $\zeta = 0.00153$ $f_n = 113.275$
$f_2 = 113.162$ B $f_1 = 113$ $\zeta = 0.00137$ $f_n = 113.31$	$f_2 = 113.137$ I $f_1 = 112.987$ $\zeta = 0.00130$ $f_n = 113.281$	$f_2 = 113.112$ P $f_1 = 112.968$ $\zeta = 0.00133$ $f_n = 113.268$	$f_2 = 113.15$ W $f_1 = 113$ $\zeta = 0.0013$ $f_n = 113.312$
$f_2 = 113.212$ C $f_1 = 113.03$ $\zeta = 0.00158$ $f_n = 113.387$	$f_2 = 113.137$ J $f_1 = 112.975$ $\zeta = 0.00144$ $f_n = 113.3$	$f_2 = 113.075$ Q $f_1 = 112.9$ $\zeta = 0.00155$ $f_n = 113.25$ SHAKER	$f_2 = 113.212$ X $f_1 = 113.037$ $\zeta = 0.00199$ $f_n = 113.487$
$f_2 = 113.125$ D $f_1 = 112.95$ $\zeta = 0.00133$ $f_n = 113.25$	$f_2 = 113.162$ K $f_1 = 113.06$ $\zeta = 0.00117$ $f_n = 113.325$	$f_2 = 113.125$ R $f_1 = 112.969$ $\zeta = 0.00138$ $f_n = 113.282$	$f_2 = 113.175$ Y $f_1 = 113.018$ $\zeta = 0.00138$ $f_n = 113.331$
$f_2 = 113.175$ E $f_1 = 113.012$ $\zeta = 0.00133$ $f_n = 113.312$	$f_2 = 113.062$ L $f_1 = 112.906$ $\zeta = 0.00134$ $f_n = 113.21$	$f_2 = 112.9$ S $f_1 = 112.73$ $\zeta = 0.00147$ $f_n = 113.062$	$f_2 = 113.175$ Z $f_1 = 113.025$ $\zeta = 0.00133$ $f_n = 113.325$
$f_2 = 113.162$ F $f_1 = 113.06$ $\zeta = 0.00119$ $f_n = 113.33$	$f_2 = 113.175$ M $f_1 = 113.018$ $\zeta = 0.00136$ $f_n = 113.325$	$f_2 = 113.15$ T $f_1 = 113.018$ $\zeta = 0.00125$ $f_n = 113.3$	$f_2 = 113.137$ AA $f_1 = 112.975$ $\zeta = 0.00144$ $f_n = 113.3$
$f_2 = 113.15$ G $f_1 = 112.98$ $\zeta = 0.00146$ $f_n = 113.31$	$f_2 = 113.1$ N $f_1 = 112.94$ $\zeta = 0.00137$ $f_n = 113.25$	$f_2 = 113.062$ U $f_1 = 112.9$ $\zeta = 0.00137$ $f_n = 113.21$	$f_2 = 113.137$ BB $f_1 = 112.98$ $\zeta = 0.00141$ $f_n = 113.3$

Table 1 shows the results of half-power point testing. Of particular note is the over-all low level of damping throughout the structure, all positions displaying less the 0.2% damping.

2. Modal Parameter Extraction

For more robust analysis of the frequency dependence of damping as well as position in the panel (and thus the wave propagation through welds) the modal parameter extraction technique was used. Similarly to the half-power point method, a 1 Volt random noise signal from the DSA was used as the input signal to the exciter. Two frequency ranges were tested, 0 to 250 Hz for a comprehensive look at vibration through the frequency range of interest and 0 to 20 Hz for a more studied examination of the lower frequencies. Frequency resolution of 0.05 Hz and 10 stable mean averages were used for both the broad band and narrow band tests. Using the National Instruments "LabView" software on the PC, five accelerometers at a time (output signals) were processed with the input signal (force sensor) to find fast Fourier transforms, calculating magnitude/phase and real/imaginary frequency response and coherence for each input/output pair. The processed fast Fourier transforms results were saved as text files for post-processing and analysis of the FFT data.

The modal parameter extraction and verification of extracted modal parameters techniques articulated in the theory section were used in a Fortan code to calculate the modal parameters of the position and regenerated the FFT curve using Microsoft Developer Studio's Fortran PowerStation 4.0. Mircocal Origin 6.0 was used to comparing the FFT curve and regenerated FFT curves. The systems most resonant modes and their associated damping were found and then saved to an Excel spreadsheet for positional comparison of frequency dependant damping. Figures 9 and 10 show an examples of resonant modes that were chosen for positional comparison.

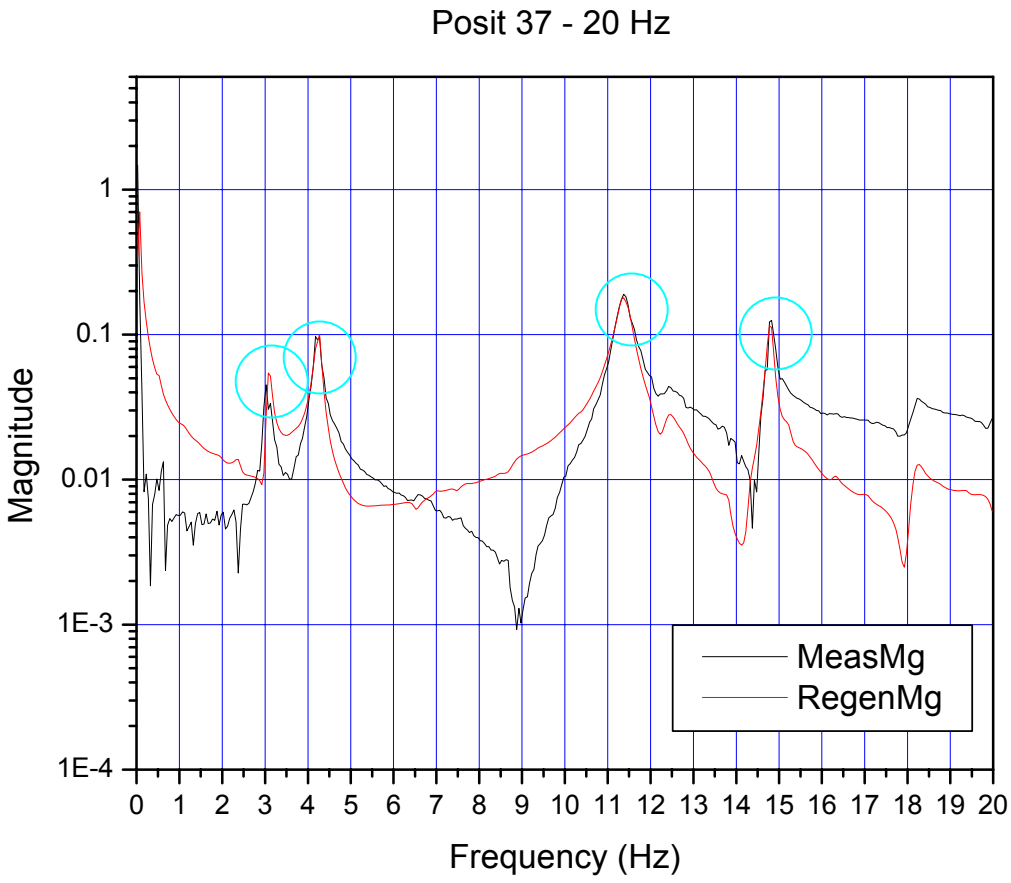

Figure 9. Sample Frequency response and Regenerated Frequency response. Circled are strongly resonant modes that would be chosen for positional comparison.

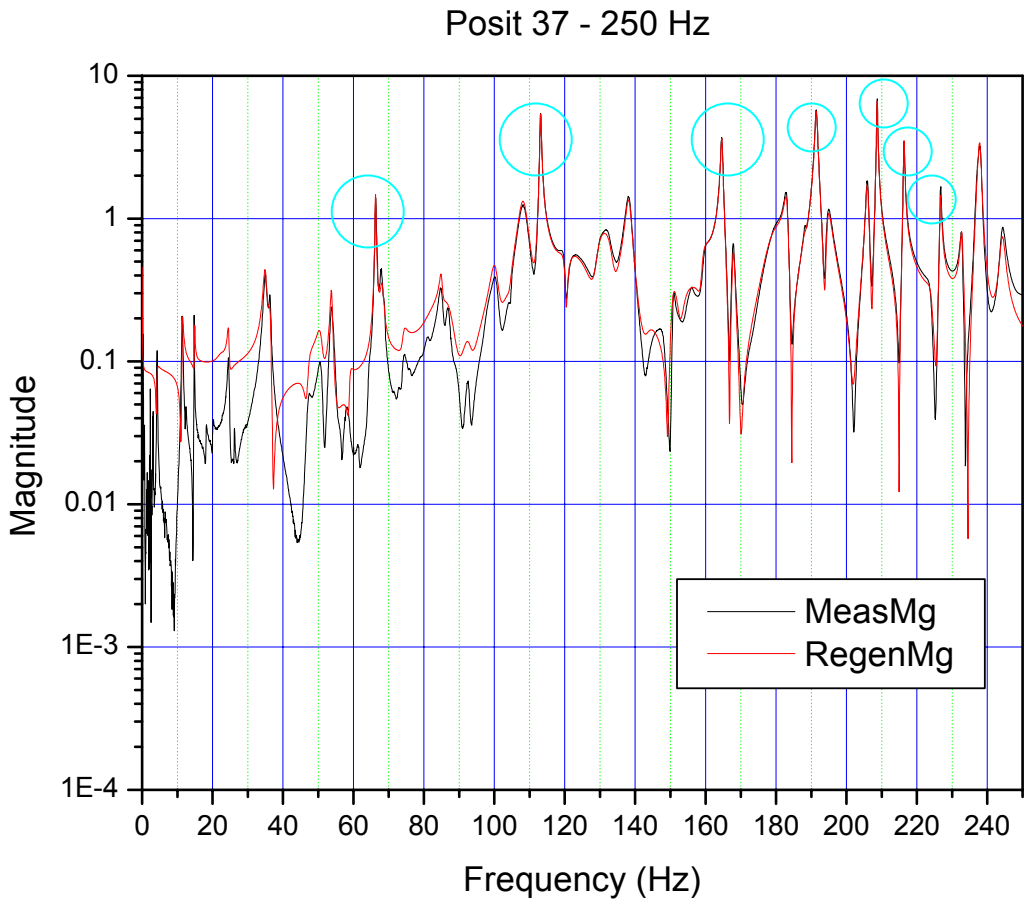

Figure 10. Sample Frequency response and Regenerated Frequency response. Circled are strongly resonant modes that would be chosen for positional comparison.

Rayleigh damping α and β for each position and the resulting curve fit was calculated as articulated in the Theory section by using the modal frequencies and damping ratios found. MATLAB code was used to use calculate these damping coefficients and to plot the curve fit compared to measured damping.

a. Horizontal Position Examination

Positional relation of damping compared horizontally from the exciter is shown in Figure 11

1	16	31	46
2	17	32	47
3	18	33	48
4	19	34	49
5	20	35	50
6	* 21	36	51
7	22	37	52
8	23	38	53
9	24	39	54
10	25	40	55
11	26	41	56
12	27	42	57
13	28	43	58
14	29	44	59
15	30	45	60

Figure 11. Horizontal Positions Compared

The testing positions along the longitudinal stiffener (Positions 7, 22, 37, and 52) and those off stiffener (Positions 6, 21, 36, and 51) were compared separately as show on figures 12 and 13 and then combined in figure 14.

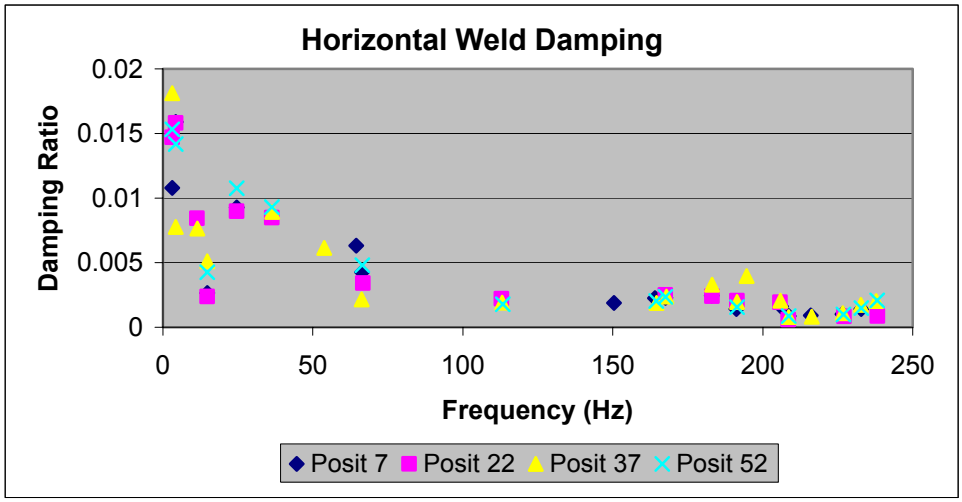

Figure 12. Horizontal Weld Damping

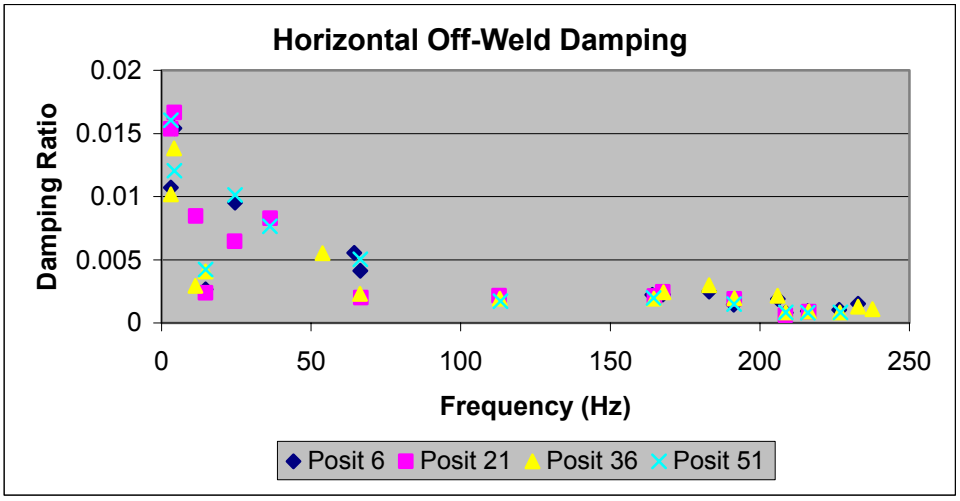

Figure 13. Horizontal Off-Weld Damping

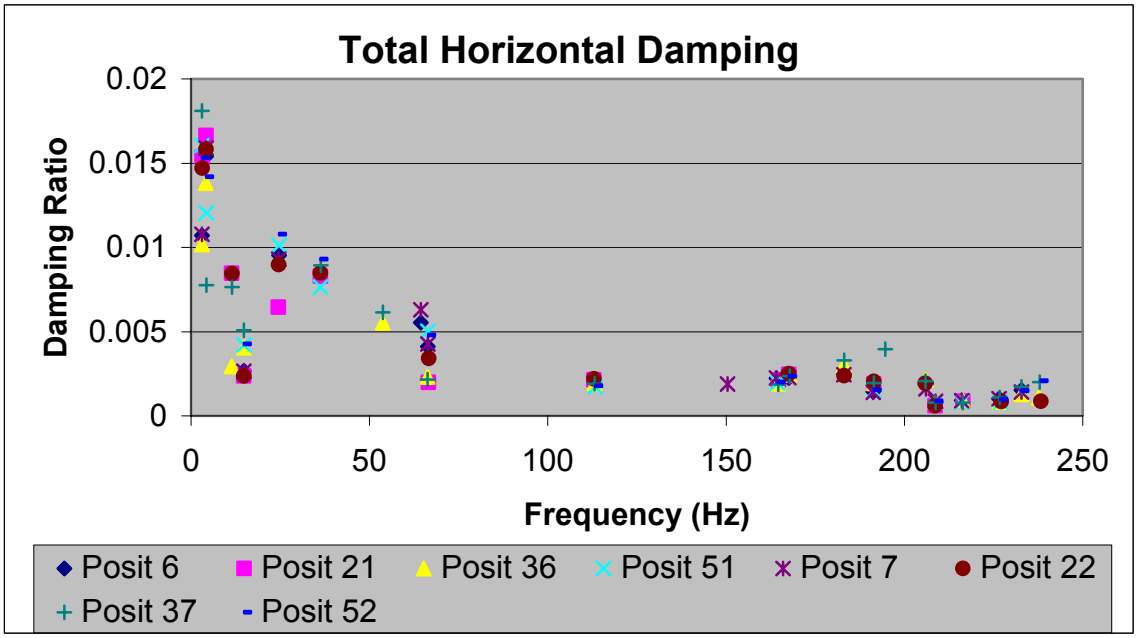

Figure 14. Total Horizontal Damping

As seen from Figures 12, 13 and 14 there is little difference in damping on or off the weld and little difference in damping in relation to testing position. Damping as a general trend however, is frequency dependant displaying an exponential decay with frequency.

The calculated Rayleigh damping α and β for each position are shown in Table 2 and the resulting curve fit compared to the original data points are shown in Figures 15, 16, 17, and 18.

Table 2. Rayleigh Damping Results for Horizontal Damping

Position	Alpha	Beta
6	0.5818	2.6823E-6
7	0.5921	2.6804E-6
21	0.7358	2.7782E-6
22	0.7163	2.6219E-6
36	0.5165	2.4298E-6
37	0.6539	3.0721E-6
51	0.6724	2.4508E-6
52	0.6947	2.8037E-6

The mean α calculated for horizontal positions was 0.6454, with a standard deviation of 0.0755 and the mean β calculated for horizontal positions was 2.6899E-6 with a standard deviation of 2.0577E-7.

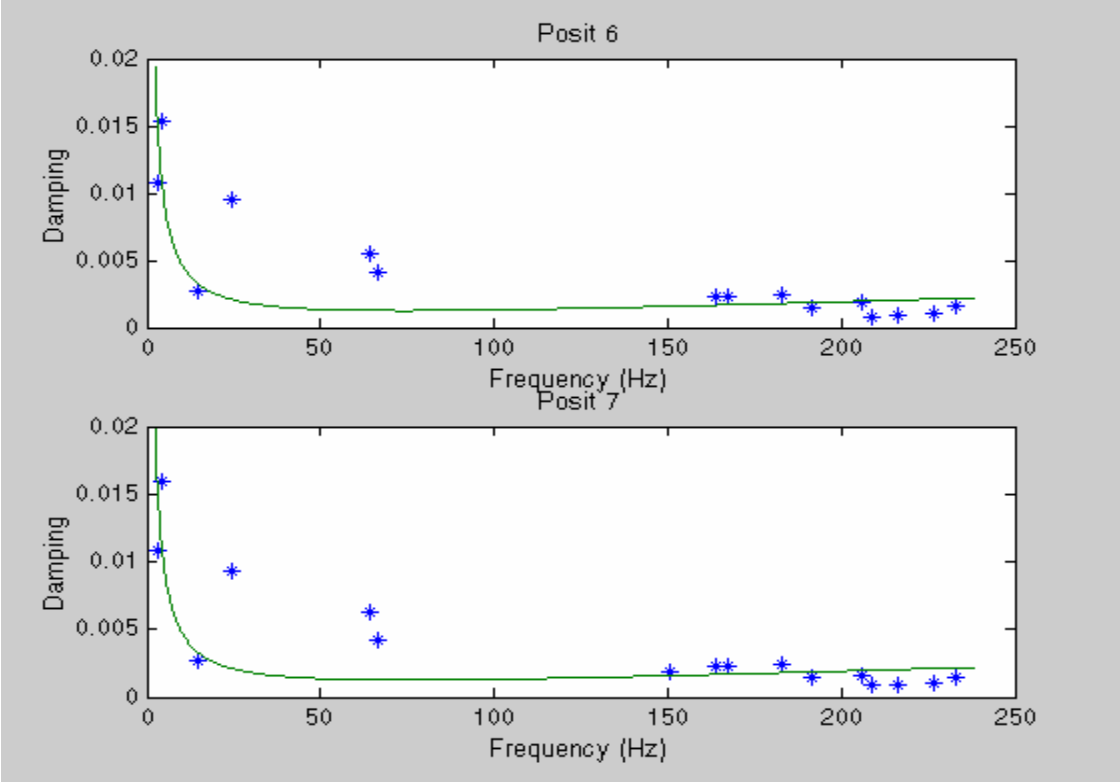

Figure 15. Positional Damping Rayleigh Damping Curve-Fit

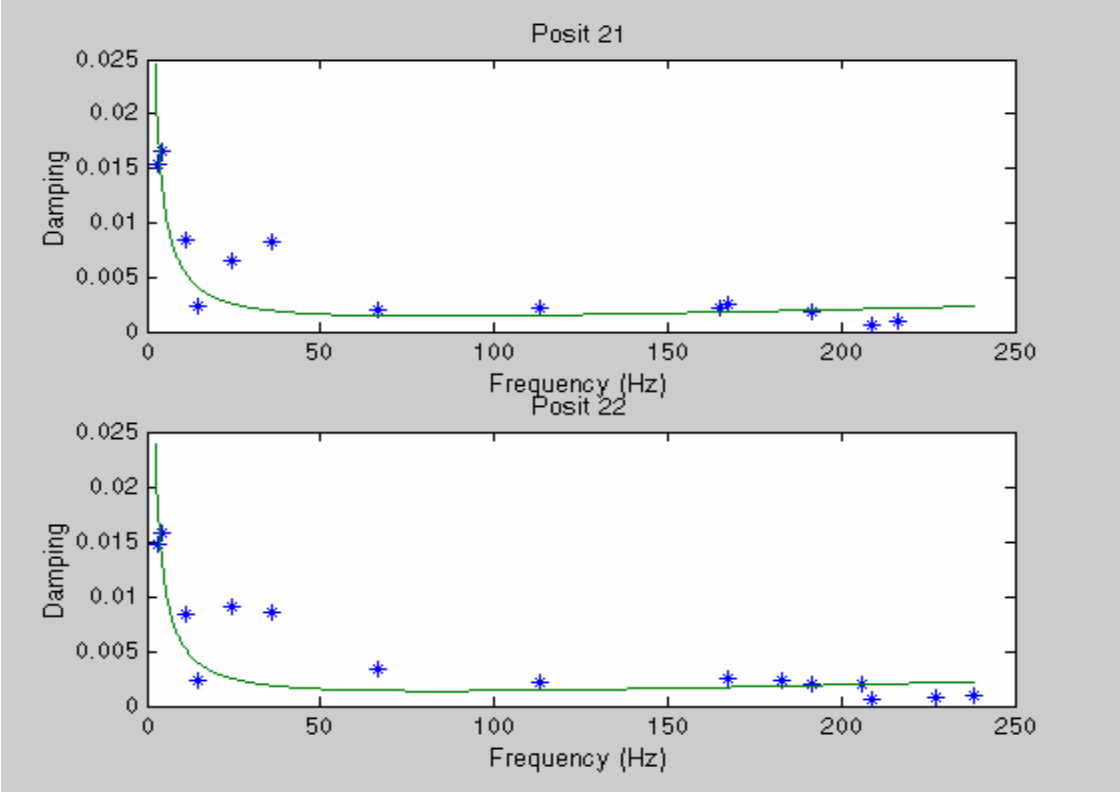

Figure 16. Positional Damping Rayleigh Damping Curve-Fit

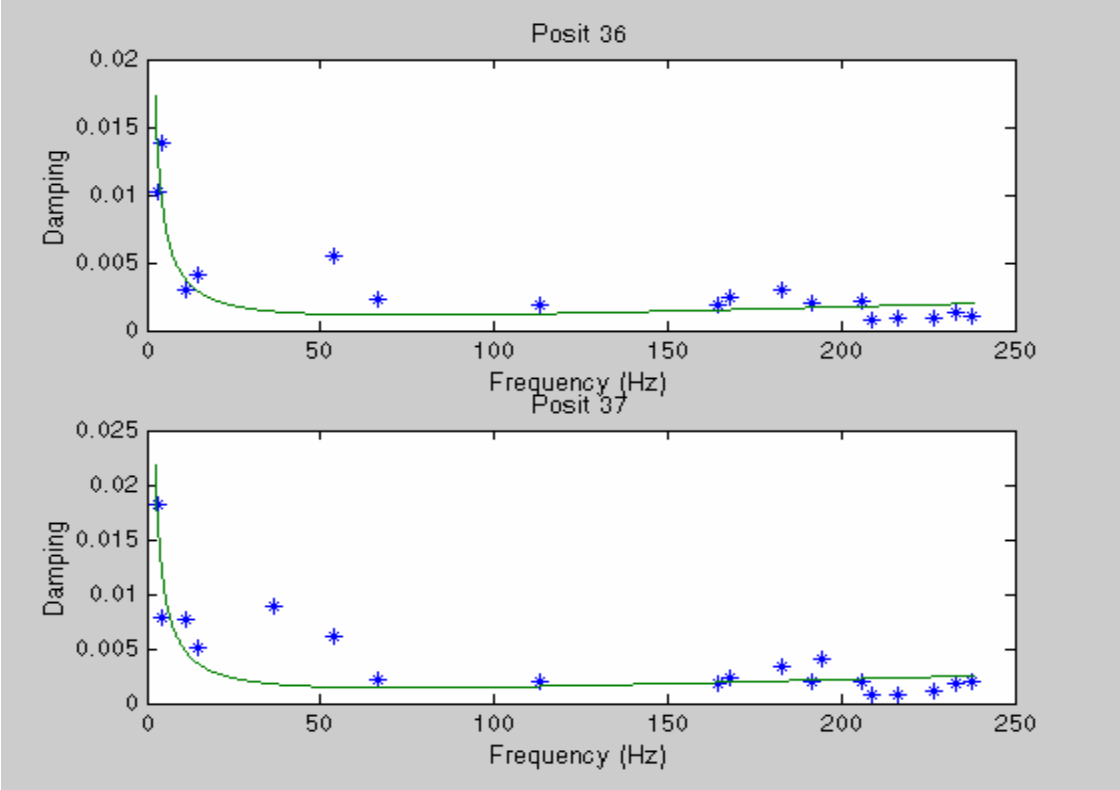

Figure 17. Positional Damping Rayleigh Damping Curve-Fit

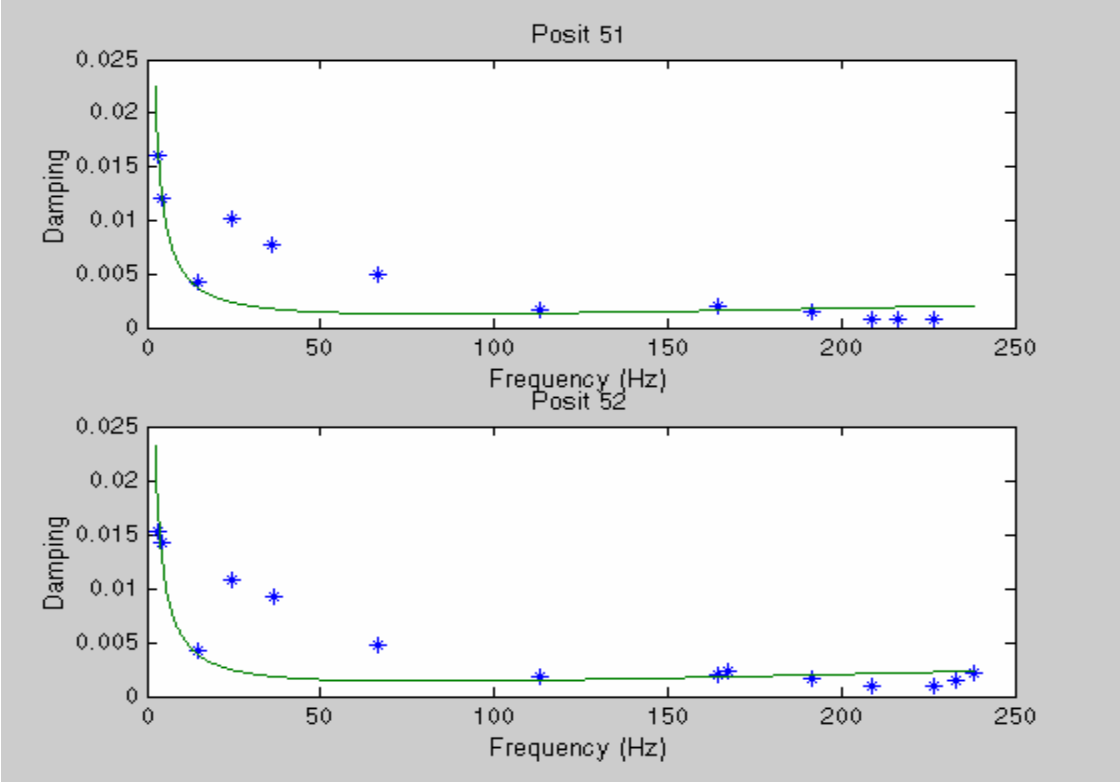

Figure 18. Positional Damping Rayleigh Damping Curve-Fit

b. Vertical Position Examination

Positional relation of damping compared vertically near the exciter is shown in figure 19.

1	16	31	46
2	17	32	47
3	18	33	48
4	19	34	49
5	20	35	50
6	* 21	36	51
7	22	37	52
8	23	38	53
9	24	39	54
10	25	40	55
11	26	41	56
12	27	42	57
13	28	43	58
14	29	44	59
15	30	45	60

Figure 19. Vertical Positions Near Exciter Compared

The vertical testing positions near the exciter (Positions 21, 22, 23, 24, 25, and 26) were compared on figure 20.

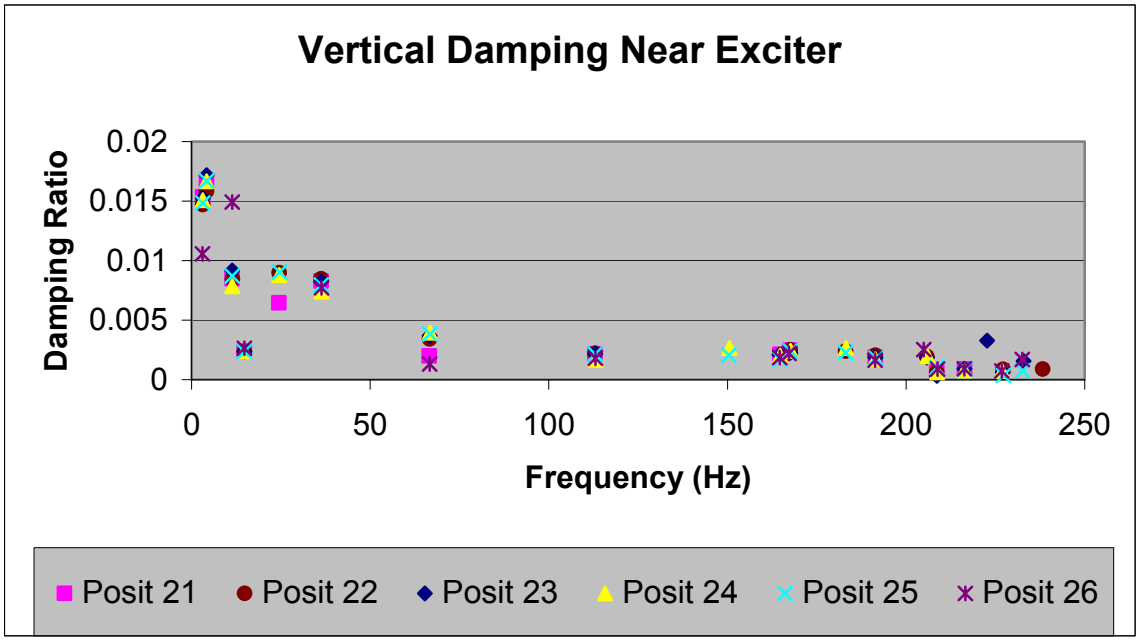

Figure 20. Vertical Damping Near Exciter

Similarly to the Horizontal position examination, figure 20 shows there is little difference in relation to testing position and damping generally displayed an exponential decay with frequency.

The calculated Rayleigh damping α and β for each position are shown in table 3 and the resulting curve fit compared to the original data points are shown in Figures 21, 22, and 23.

Table 3. Rayleigh Damping Results for Vertical Damping Near Exciter

Position	Alpha	Beta
21	0.73580	2.7782E-6
22	0.7163	2.6219E-6
23	0.7376	2.4544E-6
24	0.7332	2.7233E-6
25	0.7361	2.3462E-6
26	0.5428	2.4197E-6

The mean α calculated for vertical positions near the exciter was 0.7003 , with a standard deviation of 0.0776 and the mean β calculated for vertical positions near the exciter was 2.5573E-6 with a standard deviation of 1.7586E-7.

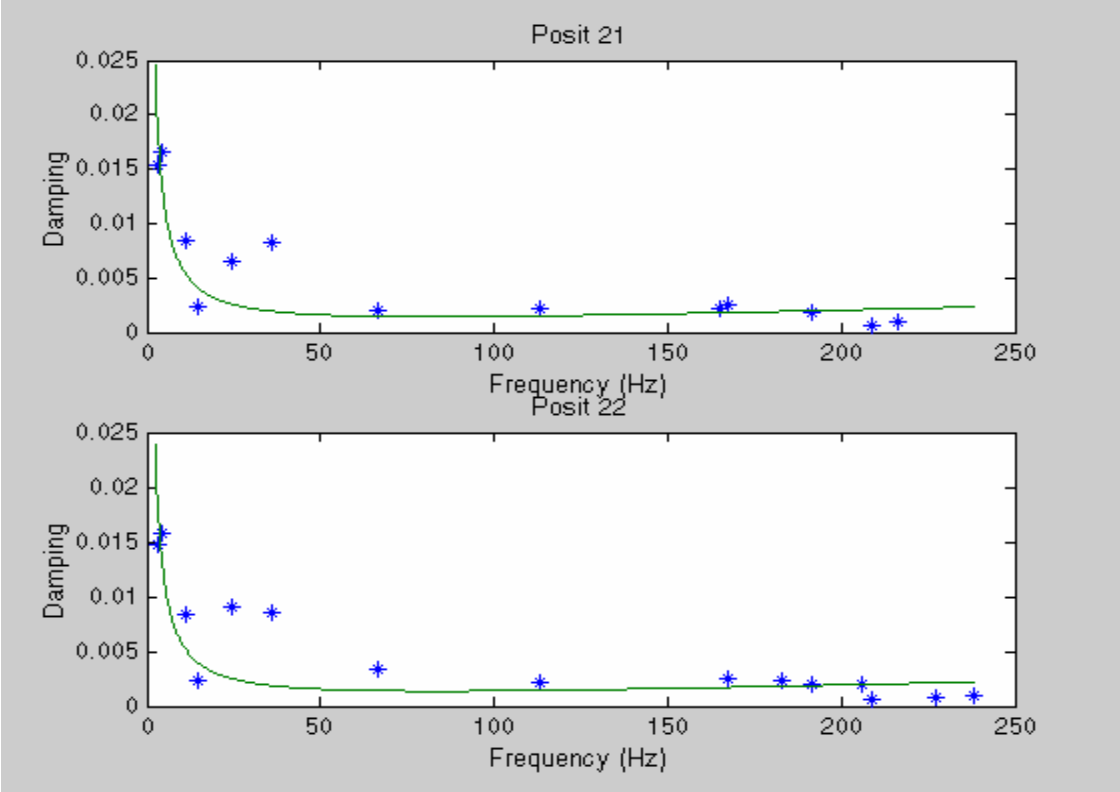

Figure 21. Positional Damping Rayleigh Damping Curve-Fit

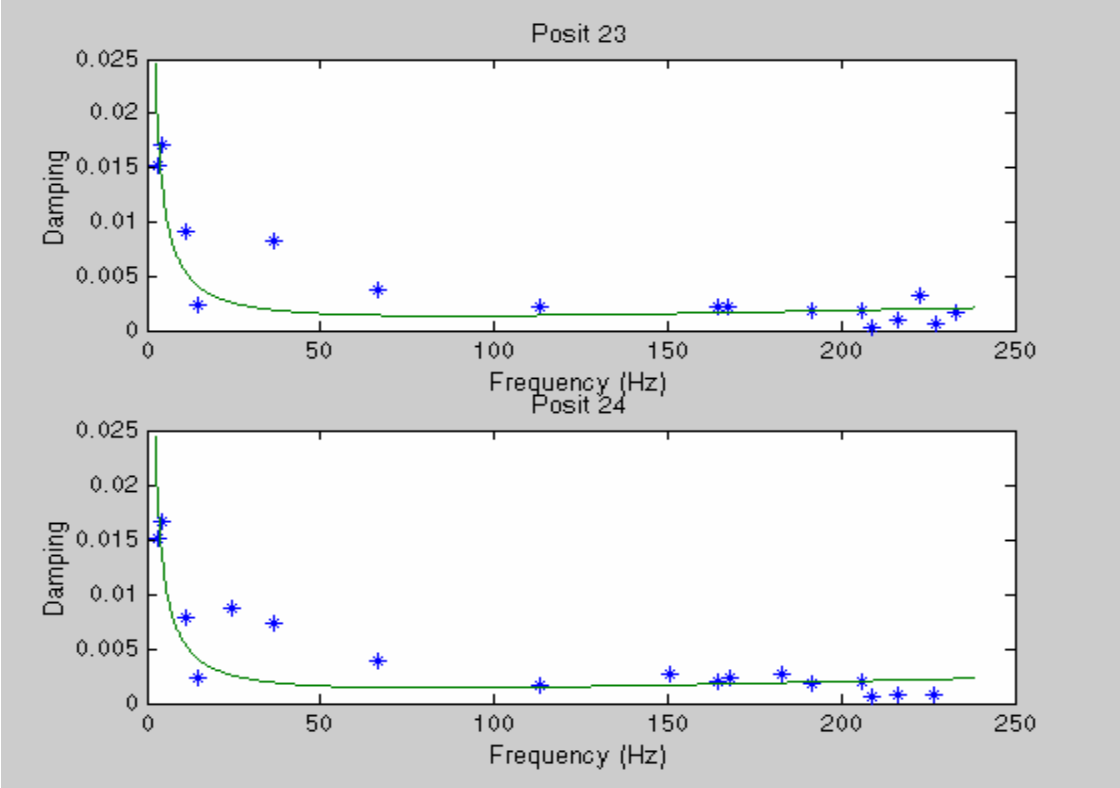

Figure 22. Positional Damping Rayleigh Damping Curve-Fit

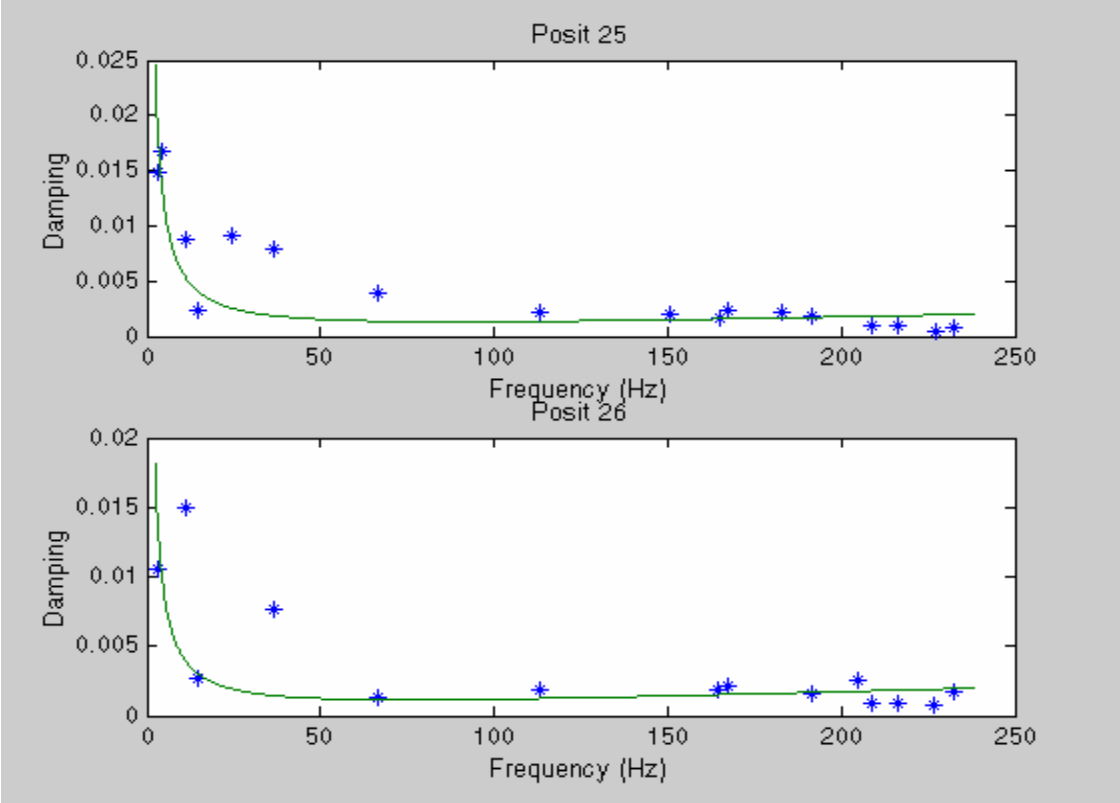

Figure 23. Positional Damping Rayleigh Damping Curve-Fit

Positional relation of damping compared vertically far from the exciter is shown in figure 24

1	16	31	46
2	17	32	47
3	18	33	48
4	19	34	49
5	20	35	50
6	* 21	36	51
7	22	37	52
8	23	38	53
9	24	39	54
10	25	40	55
11	26	41	56
12	27	42	57
13	28	43	58
14	29	44	59
15	30	45	60

Figure 24. Vertical Positions Far from the Exciter Compared

The vertical testing positions far from the exciter (Positions 51, 52, 53, 54, 55, and 56) are compared on figure 25.

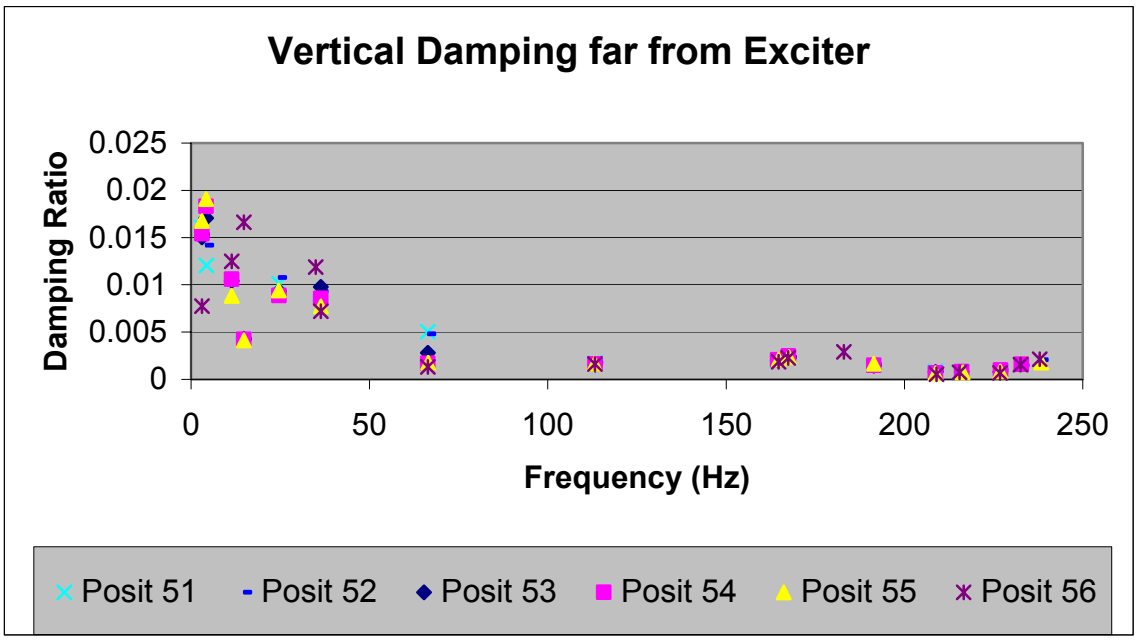

Figure 25. Vertical Damping far from Exciter

Again, similar to the horizontal position examination and the vertical positions near the exciter, figure 25 shows there is little difference in relation to testing position and damping generally displayed an exponential decay with frequency.

The calculated Rayleigh damping α and β for each position are shown in table 4 and the resulting curve fit compared to the original data points are shown in Figures 26, 27, and 28.

Table 4. Rayleigh Damping Results for Vertical Damping Far From Exciter

Position	Alpha	Beta
51	0.6724	2.4508E-6
52	0.6947	2.8037E-6
53	0.7660	2.4185E-6
54	0.7925	2.2097E-6
55	0.8263	2.1606E-6
56	0.5483	2.8479E-6

The mean α calculated for vertical positions near the exciter was 0.7167, with a standard deviation of 0.1010 and the mean β calculated for vertical positions near the exciter was 2.4819E-6 with a standard deviation of 2.8978E-7.

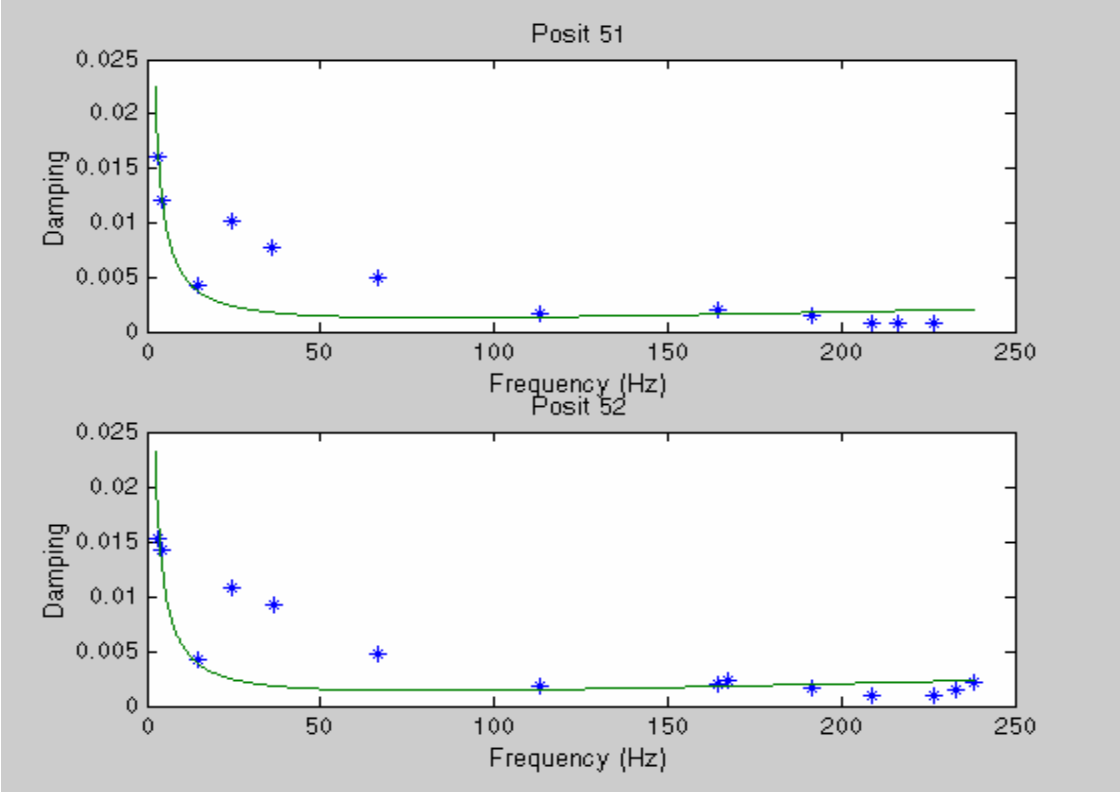

Figure 26. Positional Damping Rayleigh Damping Curve-Fit

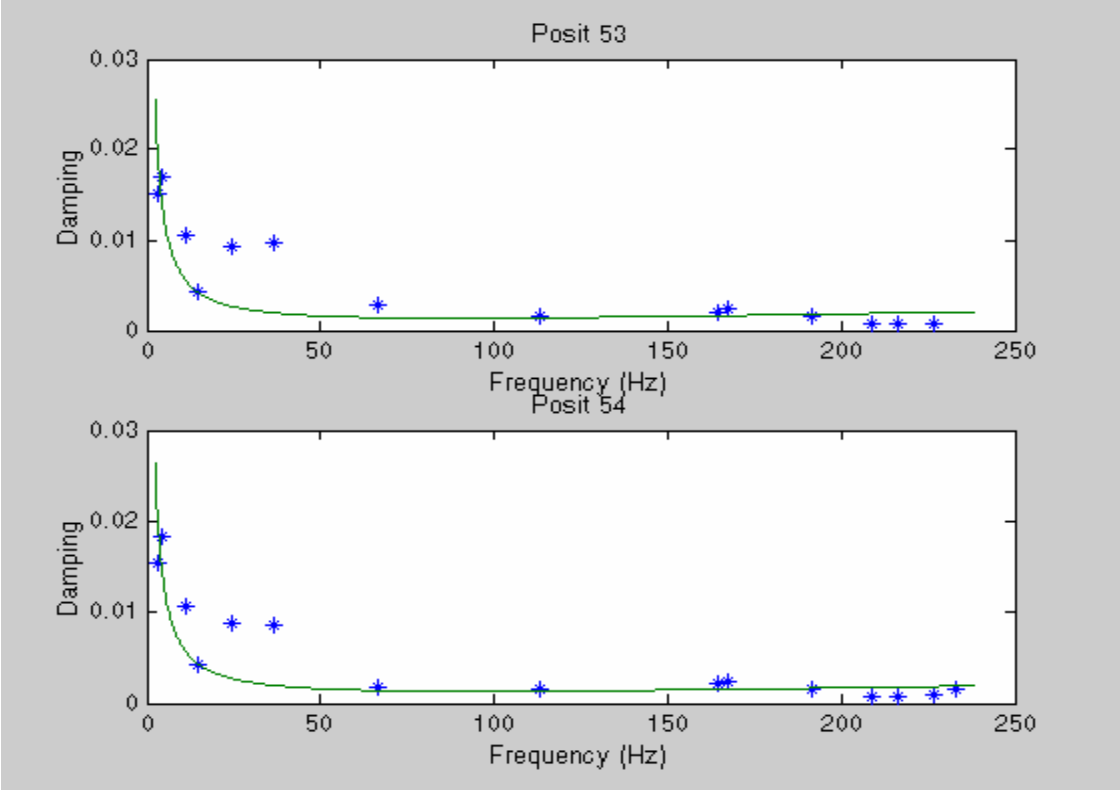

Figure 27. Positional Damping Rayleigh Damping Curve-Fit

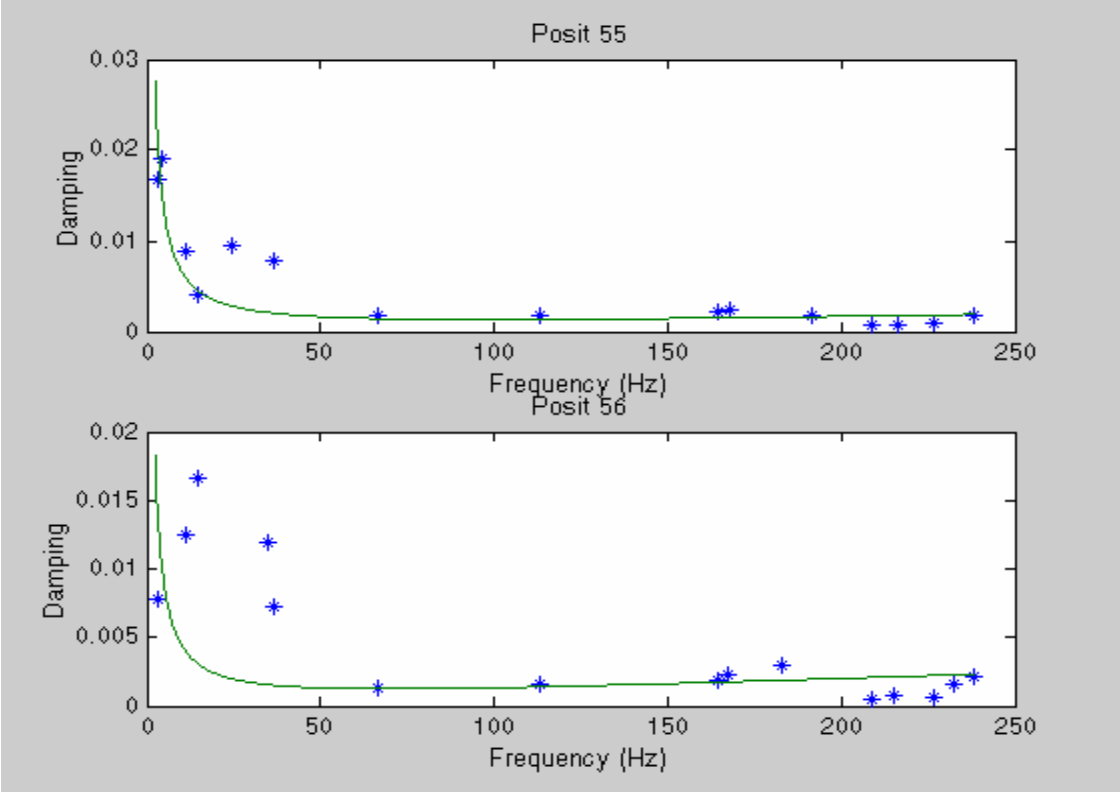

Figure 28. Positional Damping Rayleigh Damping Curve-Fit

The overall Rayleigh damping throughout the structure comparing all positions found a mean α value of 0.6779, with a standard deviation of 0.0953 and a mean β value of 2.5687E-6 with a standard deviation of 2.4747E-7.

C. FINITE ELEMENT MODELING

Using the MSC Patran/Nastran finite element modeling program, a finite element model was developed for the panel. The attempt was to observe trends that would relate the mode shape of the panel with damping and natural frequency. Table 5 shows the natural frequencies and mode shape numbers obtained from the finite element model.

Table 5. FEM Calculated Natural Frequencies

Mode	Frequency (Hz)	Mode	Frequency (Hz)
1	5.304	18	146.34
2	11.988	19	148.58
3	21.096	20	156.36
4	32.2	21	159.06
5	47.129	22	173.78
6	60.35	23	178.34
7	66.92	24	181.77

8	74.14	25	185.28
9	82.477	26	186.47
10	91.227	27	198.54
11	93.094	28	204.16
12	111.56	29	209.2
13	122.25	30	211.3
14	124.24	31	223.2
15	129.95	32	225.1
16	135.15	33	230.54
17	143.79	34	241.91

Table 6 shows FEM natural frequencies and modes that matched highly resonant experimental natural frequencies.

Table 6. Comparison of FEM and Experimental Natural Frequencies

FEM Mode Shape #	FEM Natural Frequency (Hz)	Experimental Natural Frequency (Hz)
2	11.988	11.3-11.4
3	21.096	24.4-24.6
4	32.2	36.3
7	66.92	66.3-66.6
12	111.56	112.9-113.3
24	181.77	183.0
28	204.16	205.5-206.1
29	209.2	208.5-208.9
33	230.54	232.3-232.9

Figures 29 to 33 show examples of mode shapes found by the FEM model that matched highly resonant experimental modes. Flexural (transverse and longitudinal) and torsional mode shapes as well as combination mode shapes were all found to match with highly resonant experimental natural frequencies. No type of mode shape was found to be preferential in highly resonant experimental natural frequencies.

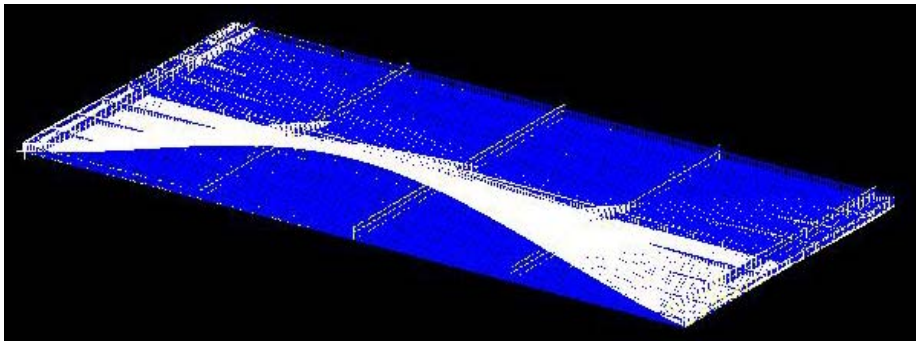

Figure 29. FEM mode shape with natural frequency of 11.988 Hz

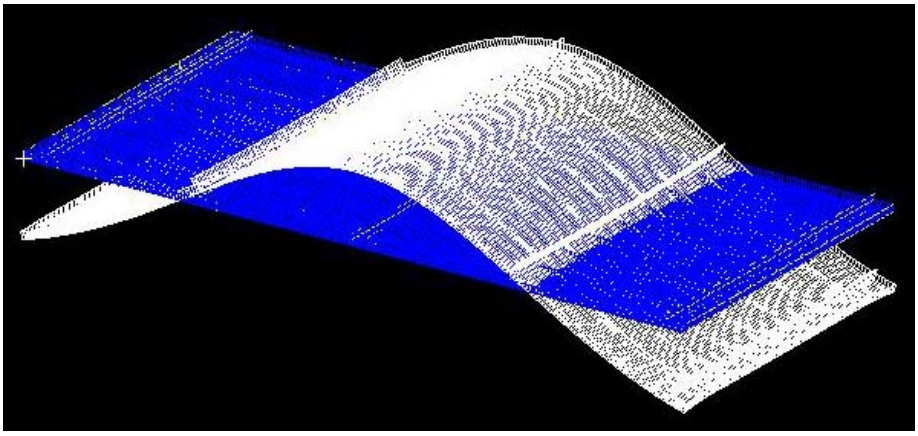

Figure 30. FEM mode shape with natural frequency of 21.096 Hz

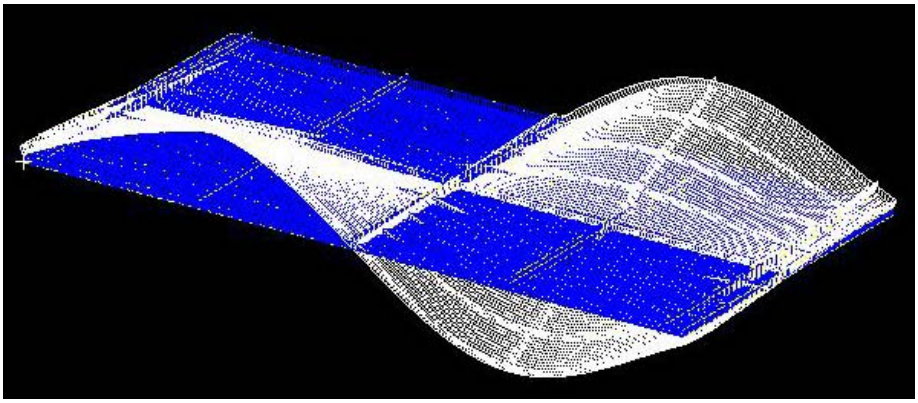

Figure 31. FEM mode shape with natural frequency of 32.2 Hz

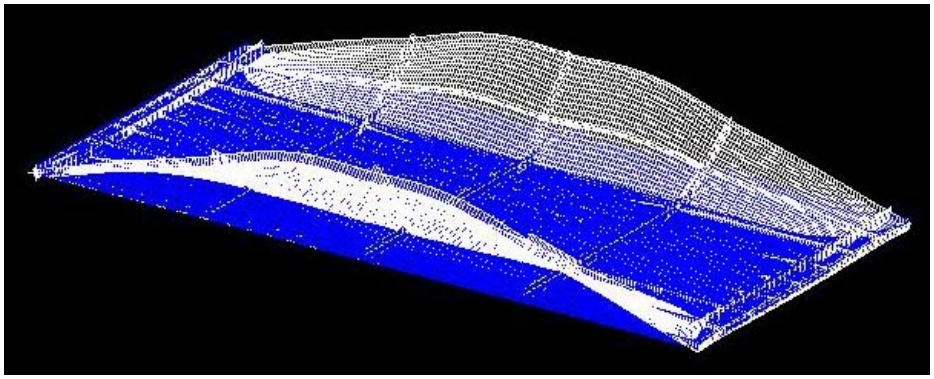

Figure 32. FEM mode shape with natural frequency of 66.92 Hz

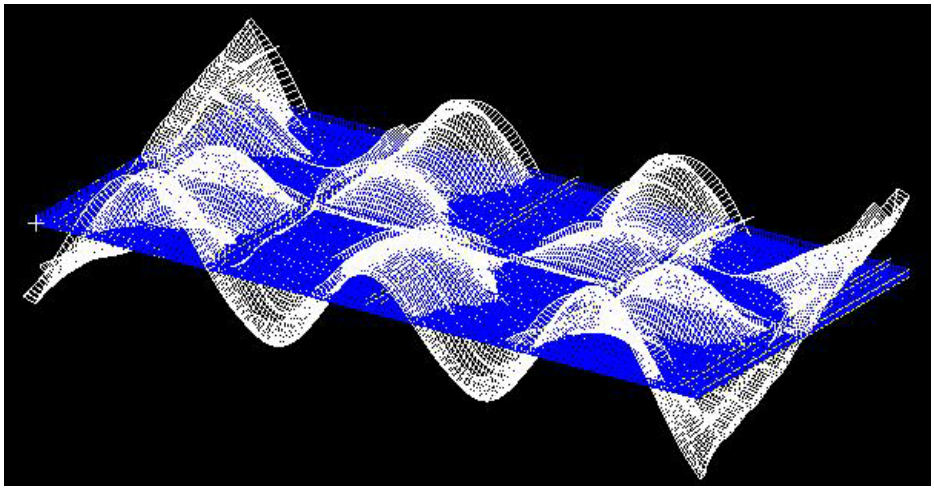

Figure 33. FEM mode shape with natural frequency of 209.2 Hz

D. FLAT PLATE COMPARISON

For reference to compare against the welded panel, the flat panel previously described in the experimental setup section was subjected to the same exciter testing and modal parameter extraction as the plate stiffened panel. Figure 29 displays the placement of the force gage and accelerometers across the panel for this testing.

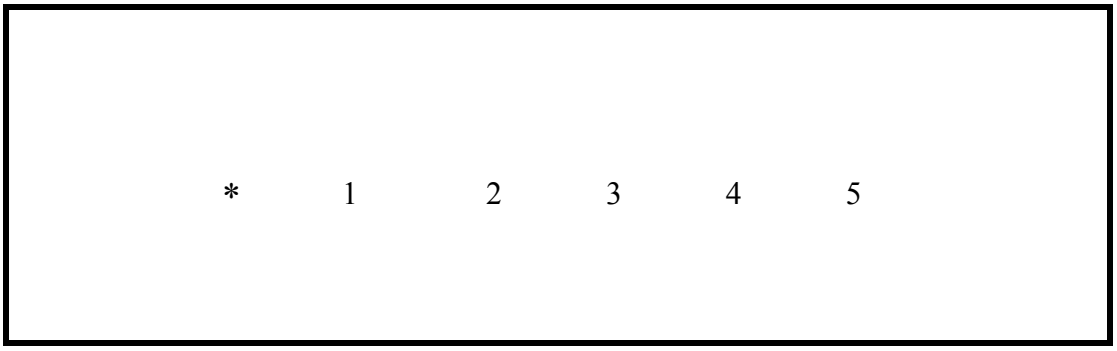

Figure 34. Exciter and Accelerometer Placement for Flat Panel Testing

The testing positions along the flat plate are compared in figure 30.

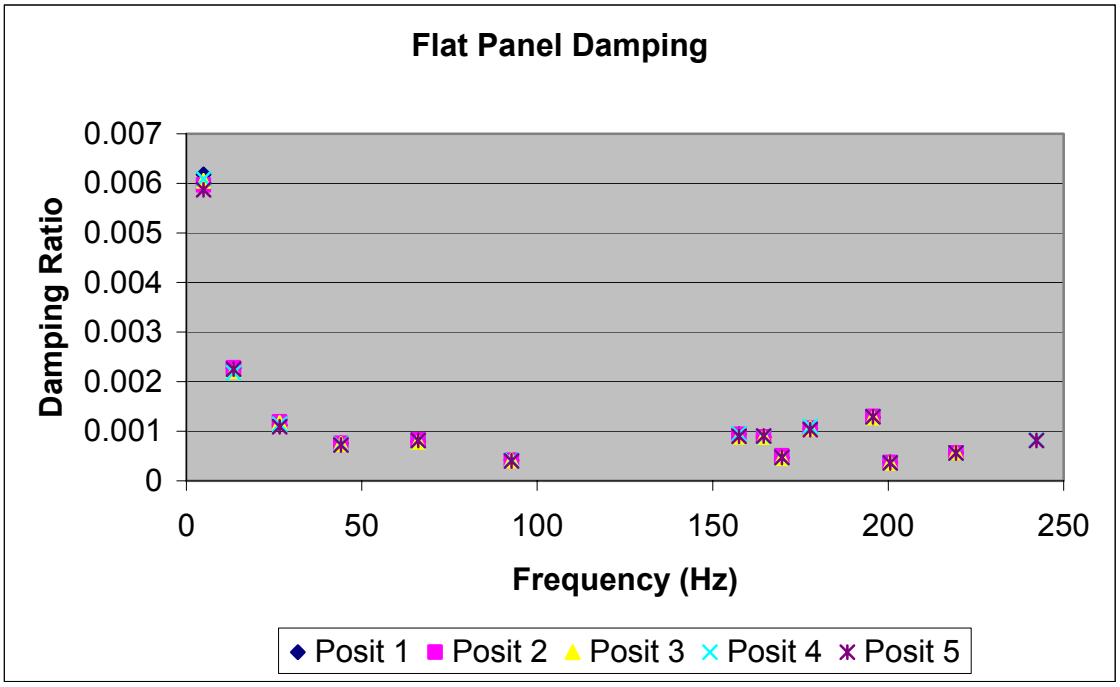

Figure 35. Flat Panel Damping

As with the plate stiffened panel, damping there appears to be little difference in relation to testing position on the flat plate and damping generally displayed an exponential decay with frequency. The difference between the flat plate and plate stiffened panel is the overall magnitude of damping for the flat plate is lower than the plate stiffened panel especially in lower frequencies (less the 50 Hz).

The calculated Rayleigh damping α and β for each position are shown in table 7 and the resulting curve fit compared to the original data points are shown in Figures 30, 31, and 32.

Table 7. Rayleigh Damping Results for Flat Plate

Position	Alpha	Beta
1	0.3797	1.0395E-6
2	0.3694	1.0657E-6
3	0.3720	1.0353E-6
4	0.3734	1.0320E-6
5	0.3628	1.0215E-6

The mean α and β calculated for horizontal positions were 0.3715 and 1.0388E-6 respectively and standard deviations of 0.0062 and 1.6451E-8. This agrees with the damping curves of figure 30, α being about 55% the value of α compared to the stiffened plate and β being about 40% the value of β compared to the stiffened pate.

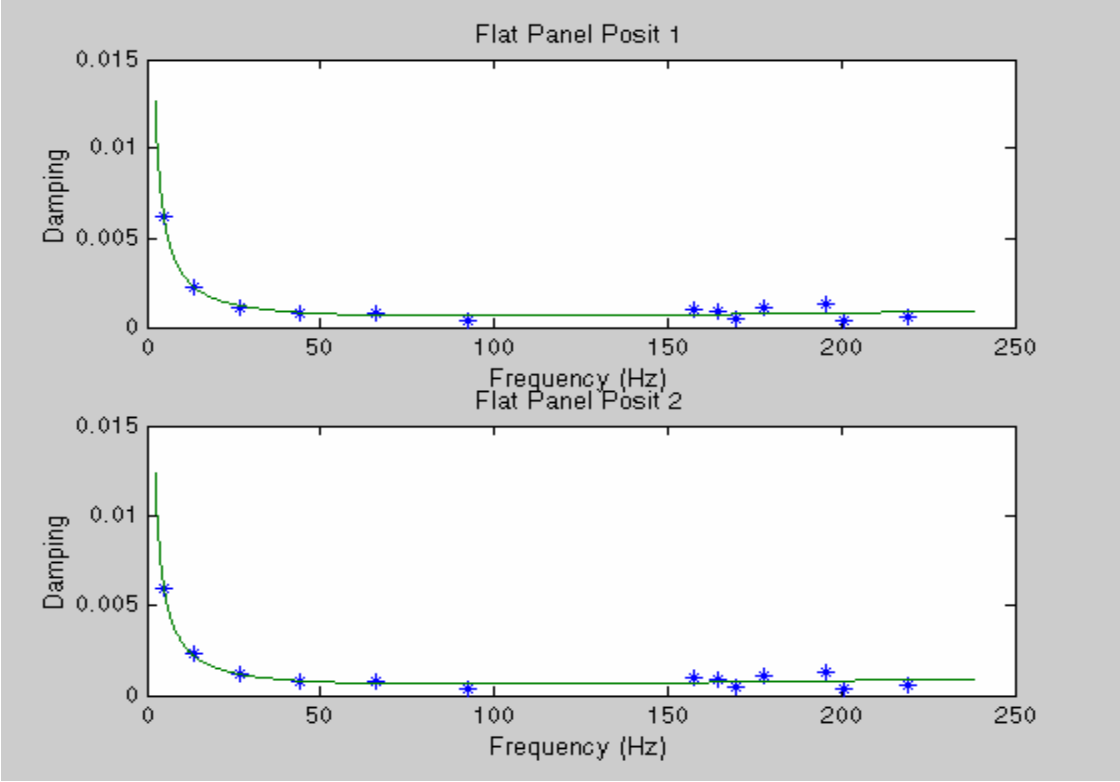

Figure 36. Positional Damping Rayleigh Damping Curve-Fit

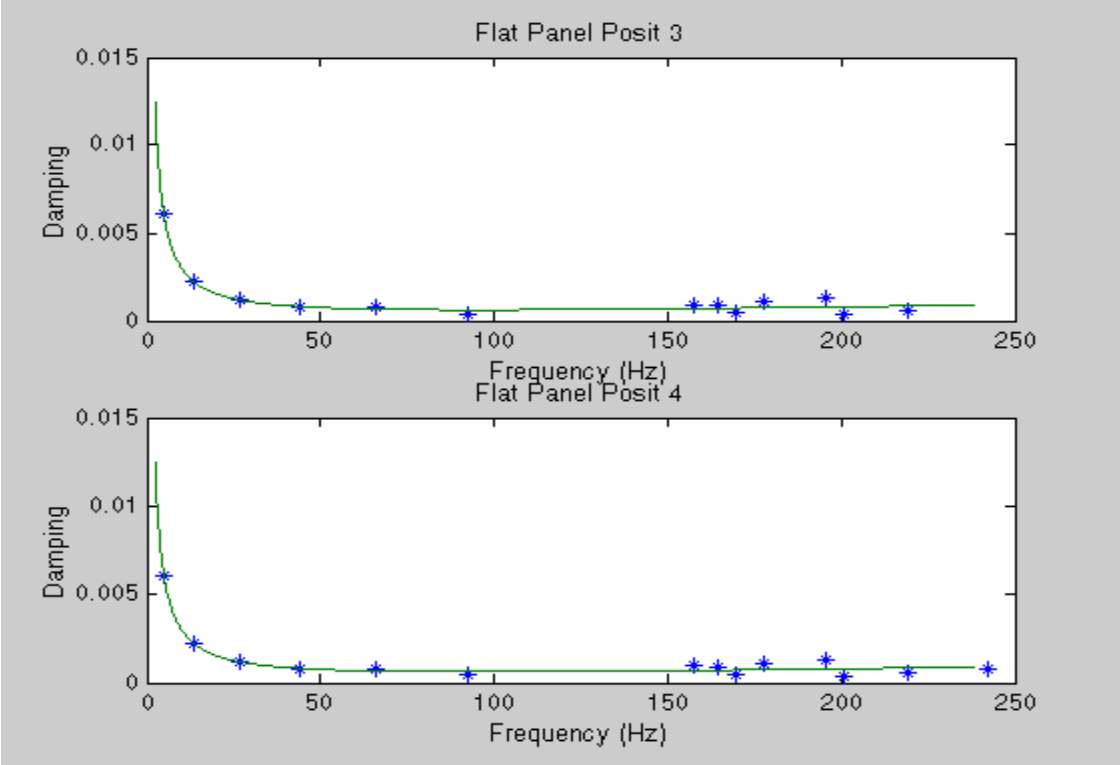

Figure 37. Positional Damping Rayleigh Damping Curve-Fit

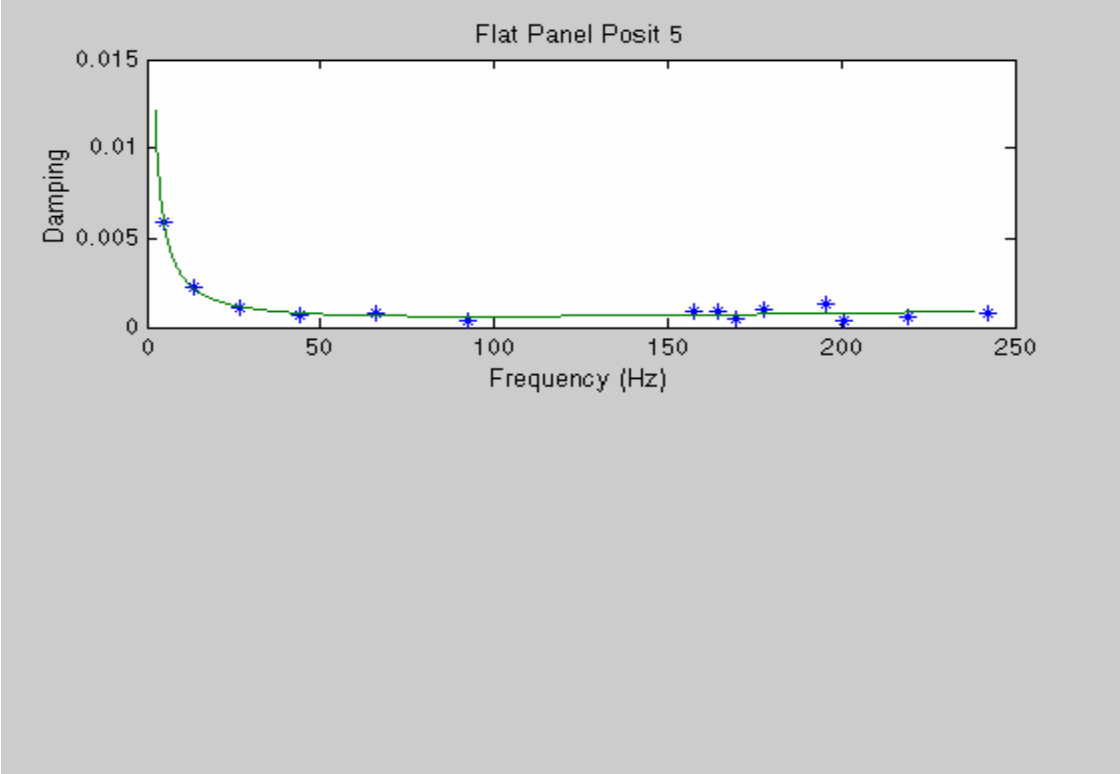

Figure 38. Positional Damping Rayleigh Damping Curve-Fit

As with the plate stiffened panel, a finite element model was developed for the flat plate in an attempt to observe trends relating the mode shape of the panel with damping and natural frequency. Table 8 shows the natural frequencies and mode shape numbers obtained from the finite element model.

Table 8. FEM Calculated Flat Plate Natural Frequencies

Mode	Frequency (Hz)	Mode	Frequency (Hz)
1	4.913	13	124.25
2	13.596	14	152.84
3	16.821	15	158.16
4	26.772	16	164.4
5	34.338	17	169.77
6	44.436	18	178.29
7	53.20	19	185.94
8	66.603	20	196.43
9	73.988	21	201.41
10	93.247	22	219.41
11	97.22	23	222.93
12	123.38	24	243.22

Table 9 shows FEM natural frequencies and modes that matched highly resonant experimental modes.

Table 9. Comparison of Flat Plate FEM and Experimental Natural Frequencies

FEM Mode Shape #	FEM Natural Frequency (Hz)	Experimental Natural Frequency (Hz)
1	4.913	4.92
2	13.596	13.45
4	26.772	26.55
6	44.436	44.07
8	66.603	66.13
10	93.247	92.71
15	158.16	157.48
16	164.4	164.49
17	169.77	169.67
18	178.29	177.83
20	196.43	195.62
21	201.41	200.55
22	219.41	219.27
24	243.22	242.26

The modes and frequencies of the FEM model closely matched all resonant modes of the flat plate found experimentally and only a few "false" modes were created by the FEM model. This result confirmed the veracity of the FEM model but added no further insights into the relationship between welds and damping.

THIS PAGE INTENTIONALLY LEFT BLANK

V. CONCLUSIONS AND RECOMENDATIONS

The results of this damping study indicate that welds do increase the damping of structure and that Rayleigh damping is and appropriate model for its analysis. The study results indicate that damping is relatively high in the low frequency domain while decreasing exponentially in the higher frequencies. The damping from the welds increased the damping of the overall system but did not show any positional damping. Damping values found near the point of excitation were similar to damping values of positions separated from the point of excitation by multiple welds.

This level of damping increase found compare to a bare, flat plate however is extremely small, with average Rayleigh damping coefficients of $\alpha = 0.6779$ and $\beta = 2.5687\text{E-}6$ found. From DDG-53 ship shock trial data, Rayleigh damping coefficients of $\alpha = 19.2$ and $\beta = 2.09\text{E-}6$ were estimated for ship structural damping. [Ref. 9] The minor increase in damping found due to welds in this study is unlikely to be a significant contributor to overall this ship structure damping found.

Recommendations for future work into the study of the sources ship structural damping would be to attempt to find the damping effects of painting and lagging on the ship structure.

THIS PAGE INTENTIONALLY LEFT BLANK

VI. LIST OF REFERENCES

1. Betts, C. V., R. E. D. Bishop and W.G. Price, The Royal Institution of Naval Architects. 1976 "A Survey of Internal Hull Damping."

2. Carey, A. E., 2002 Thesis, Naval Post Graduate School. "Experimental Studies of Welding Effects on Damping for Undersea Warfare Applications."

3. Thomson, W.T. and M.D. Dahleh, Theory of Vibration With Applications, 5th Ed., Prentice-Hall Inc., 1998.

4. Craig, R. R., Structural Dynamics, An Introduction to Computer Methods, John Wiley & Sons, Inc., 1981.

5. Ewins, D.J., Modal Testing: Theory and Practice, Research Studies Press Ltd., 1984.

6. Hewlett-Packard Co. 3562A Dynamic Signal Analyzer Operating Manual, Hewlett-Packard Co., 1985.

7. PCB Piezotronics Model 208C01 ICP Quartz Force Sensor Installation and Operating Manual (Manual 18218), 2002.

8. PCB Piezotronics Model 208C01 ICP Quartz Force Sensor Calibration Certificate, 2002.

9. Shin, Y.S., "Damping Modeling Strategy for Naval Ship Systems", Report NPS-ME-03-003, Naval Postgraduate School, May 2003.

THIS PAGE INTENTIONALLY LEFT BLANK

INITIAL DISTRIBUTION LIST

1. Defense Technical Information Center
   Ft. Belvoir, Virginia

2. Dudley Knox Library
   Naval Postgraduate School
   Monterey, California

3. Young S. Shin
   Naval Postgraduate School
   Monterey, California

4. Ilbae Ham
   Naval Postgraduate School
   Monterey, California

5. Fred Costanzo
   NSWC Carderock Division
   Washington, DC

6. Mike Campbell
   NSWC Carderock Division
   Washington, DC

7. Steve Rutgerson
   NSWC Carderock Division
   Washington, DC

8. Charles Ehnes
   Naval Postgraduate School
   Monterey, California